Exploring Mechanocardiography as a Tool to Monitor Systolic Function Improvement with Resynchronization Pacing

University of Turku
Department of Computing
Master of Science Thesis
Digital Health Technology
March 2024
Fadime Tokmak

UNIVERSITY OF TURKU
Department of Computing

Fadime Tokmak: Exploring Mechanocardiography as a Tool to Monitor Systolic Function Improvement with Resynchronization Pacing

Master of Science Thesis, 51 p.
Digital Health Technology
March 2024

The thesis explores the utilization of mechanocardiography (MCG) as a novel approach to assess and quantify improvements in systolic cardiac function resulting from cardiac resynchronization therapy (CRT). The study focuses on patients with heart failure and reduced ejection fraction (HFrEF), a population commonly treated with CRT. The primary objective is to investigate the differences in MCG waveforms during CRT and single-chamber atrial (AAI) pacing, specifically comparing waveform characteristics. 10 patients with heart failure and previously implanted CRT pacemakers were included in the study. The MCG and ECG signals are recorded using accelerometers, gyroscopes, and Holter measurement unit placed on the lower chest and used in the analysis. ECG and MCG recordings were obtained during both CRT and AAI pacing at a consistent heart rate of 80 beats per minute. The analysis involved considering six MCG axes and three MCG vectors across various frequency ranges to derive key waveform characteristics such as energy, vertical range, electromechanical systole (QS2), and left ventricular ejection time (LVET). The results revealed significant differences between CRT and AAI pacing, with CRT consistently exhibiting higher energy and vertical range during systole across multiple axes. Notably, the study identified optimal differences in SCG-Y, GCG-X, and GCG-Y axes within the 6–90 Hz frequency range. However, any difference in QS2, LVET and waveform characteristics around aortic valve closure was not identified between the pacing modes.

The findings suggest that MCG waveforms can serve as indicators of improved mechanical cardiac function during CRT. The use of accelerometers and gyroscopes may contribute to the development of a non-invasive and potentially predictive tool for optimizing CRT settings. The promising results underscore the need for further research to explore the differences in signal characteristics between responders and nonresponders to CRT. The overall aim is to enhance the clinical application of MCG, leveraging wearable technology and micro-electromechanical systems (MEMS), and ultimately improve the optimization and efficacy of CRT in heart failure (HF) management.

Keywords: accelerometer, gyroscope, heart failure, resynchronization therapy, smartphone

Contents

List of Figures

List of Tables

1 Introduction

Cardiovascular disease (CVD) poses a common and complex public health challenge, with a prevalence of 48.6% in adults aged 20 years and older and impacting 127.9 million individuals in 2020 in United States only [1], [2]. This prevalence rises with age in both males and females, and it includes conditions such as coronary heart disease (CHD), heart failure (HF), stroke, and hypertension [3]. Excluding hypertension, the overall CVD prevalence is 9.9% [2]. Significantly, long-term fatal CVD risks are associated with male gender, older age, and smoking, based on current literature [4].

Heart Failure (HF) is a complex clinical syndrome characterized by the inability of the heart to pump blood efficiently and leads to insufficient oxygen supply to meet the body's needs [5]. According to data from NHANES (2017-2020), approximately 6.7 million Americans aged 20 and above had HF, with a projected increase to over 8 million by 2030 [2]. The prevalence of HF is expected to rise by 46% from 2012 to 2030 in the population, including individuals aged 18 and above [6].

Various factors contribute to the development of HF, including cardiometabolic factors such as CHD, hypertension, diabetes, obesity, and smoking [7]. The lifetime risk of HF increases with age [8]. The mortality associated with HF has improved, primarily due to evidence-based treatments for HF with reduced ejection fraction (HFrEF) [9]. HF causes a significant economic burden, with high rates of hospitalizations, emergency department visits, and resulting costs [6]. Improving risk factor

management and following evidence-based treatments are crucial in addressing the growing burden of HF.

Cardiac resynchronization therapy (CRT) devices can be used to manage HF [5], [10], [11]. They are connected to the heart with three wires. They aim to enhance ventricular activation, detect heart irregularities, and correct them with electrical pulses, resulting in improved cardiac function [11], [12]. Supported by extensive clinical trials, CRT is beneficial for moderately and severely symptomatic HF patients.

In individuals with sinus rhythm, low ejection fraction (EF $\leq$ 35%), and QRS duration of $\geq$ 120 ms (preferably with left bundle branch block morphology), CRT is recommended for those who are expected to survive with good functional status for over a year and aims to reduce the risk of HF hospitalization and premature death [13]–[15]. It has been shown that it is effective in improving symptoms, quality of life, and ventricular function and is a valuable option in the management of heart failure.

Clinical trials evaluating CRT effectiveness in diverse patient groups have shown significant recovery and reverse remodeling in the majority of heart failure (HF) patients, but about one-third do not respond positively [16]. Accordingly, the CRT management process involves crucial follow-up stages to identify factors predicting positive outcomes and address non-responders [17]. Assessing CRT response includes measures like left ventricle volumetric changes, quality of life assessments, and functional capacity evaluations [17]–[19].

Seismocardiography (SCG) was first introduced by Salerno et al. in 1990 as a noninvasive displacement cardiography technique [20]. SCG is a technique based on 3-axis accelerometers placed on the sternum, and it aims to capture vibrations resulted by cardiac contraction, hemodynamic activity, and valve movements [21]. Gyrocardiography (GCG) is another technique invented by Meriheinä et al. [22]

and uses a gyroscope to capture three-dimensional angular velocity on the sternum, providing information about cardiac vibrations [23]. Mechanocardiogram (MCG) is a methodology that includes both SCG and GCG complementarily to acquire 6-axis information regarding heart vibrations [24].

The increasing popularity of smart mobile devices, equipped with 3-axis accelerometers and gyroscopes, has made SCG and GCG promising monitoring techniques. Together, they form MCG, which can be gathered in home settings, offering a potential avenue for remote monitoring of individuals with cardiological conditions. Literature demonstrates that these vibrations contain crucial information about cardiac time intervals, cardiac performance, hemodynamic variables, and heart diseases [25]–[28].

Existing studies have showed the potential usefulness of MCG in identifying atrial fibrillation, aortic stenosis, and evaluating conditions associated with cardiac resynchronization therapy, heart failure, and myocardial infarction [26], [29]–[33]. Increasing evidence supporting the utility of MCG for heart monitoring holds promise for its application in patient selection, optimization, and follow-up procedures for CRT.

1.1 Research questions

This study focuses on the effect of CRT on MCG waveforms by comparing waveform features during AAI (single chamber) and CRT (dual chamber) pacing. We aim to address the following research questions in evaluating the waveform characteristics during CRT and AAI pacing using MCG signals:

- Are there differences in MCG waveform characteristics that are consistently observable between CRT and AAI pacing modes in patients with HFrEF?
- Which cardiac events show differences following the initialization of CRT

mode?

- Do specific MCG axes and frequency ranges provide differentiation between CRT and AAI pacing?
- Are there any significant changes in timing parameters, including electromechanical systole (QS2) and left ventricular ejection time (LVET), between CRT and AAI pacing?
- How do different synchronization methods, such as R-peak and AO point synchronization, impact the analysis of MCG signals in assessing mechanical cardiac function during CRT and AAI pacing?

The results of this study contribute to understanding the potential of MCG in detecting and assessing improvements in cardiac mechanical function during CRT. The findings may have implications for predicting clinical response to CRT and optimizing pacing settings for patients with HFrEF.

1.2 Contributions

In this study, we present a comprehensive investigation of the waveform characteristics during CRT and AAI pacing using MCG signals in patients with HFrEF. The primary contributions of this study are as follows:

- A detailed analysis of waveform features, focusing on energy and vertical range during systole and early diastole was conducted. It is shown that energy and range during systole significantly differ between CRT and AAI pacing, reflecting improved systolic performance caused by resynchronization of ventricles.
- QS2 and LVET during CRT and AAI pacing were extracted to compare the timing parameters associated with these pacing modes.

- Specific MCG axes and frequency ranges that exhibit optimal differences between CRT and AAI pacing modes were identified. These findings contribute to understanding which parameters are most informative in reflecting the improvements.

- The impact of different synchronization methods, including R-peak and AO point synchronization, on the analysis of MCG signals was evaluated. This provided valuable insights into the robustness and consistency of MCG analysis under varying synchronization conditions.

- Analysis of the MCG signals while also incorporating the SCG, GCG, and MCG vectors was conducted. A new algorithm for MCG vector extraction, accounting for potential range variations between SCG and GCG measurement units was introduced.

- To address the constraints of a limited patient cohort and account for time-dependent differences in the analysis, a specialized data analysis algorithm is introduced.

In summary, this study provides a novel way for mechanical cardiac function assessment during different pacing modes and offers new insights for future investigations in optimizing CRT for patients with HFrEF. This thesis is connected to the accepted publication [34].

1.3 Thesis content summary

Later sections of the thesis are structured as follows: Chapter 2 offers the background, covering topics such as heart failure (HF), cardiac resynchronization therapy (CRT), mechanocardiography (MCG), electrocardiogram (ECG), and statistical hypothesis testing. Chapter 3 delves into related work, exploring filtering of MCG

signals, fiducial point detection on MCG signals, and assessment of cardiac function with MCG signals. Chapter 4 provides information on the MECHANO-HF dataset, while Chapter 5 outlines our proposed method in detail, including signal processing, feature extraction, and statistical tests. Chapter 6 presents the results and Chapter 7 provides a thorough discussion of the findings. Finally, Chapter 8 concludes the thesis.

2 Background

2.1 Heart Failure (HF)

Heart failure (HF) is a leading cause of death worldwide and is a syndrome in which the heart loses its ability to maintain ventricular filling and expulsion of blood at the level required for metabolic needs [5]. HF causes physical symptoms like shortness of breath, fatique, edema and chest pain [35], [36]. The decrease in the cardiac performance is related with the loss of functional myocardial cells and etiology of the loss can be various [37]. The severeness of loss in the cardiac output is important information that affects to the prognosis and treatment of heart failure patients which are classified according to their left ventricular ejection fraction (LVEF) as HFrEF, HFimpEF, HFmrEF, HFpEF (from the highest loss to lowest loss) [5]. Patients with HFrEF have 40% or lower LVEF which means heart is capable to eject only 40% or less of the blood filled during diastole to the ventricles [38].

In addition to the classification based on LVEF, it is essential to consider the underlying causes of heart failure for a comprehensive treatment approach. The etiology of heart failure can be diverse, including ischemic heart disease, hypertension, valvular disorders, and inflammatory cardiomyopathies, among others [37]. Tailoring treatment to address the specific underlying cause is crucial for optimizing patient outcomes. Furthermore, the presence of accompanying cardiac abnormalities, such as mechanical and electrical dyssynchrony, necessitates specialized

interventions. In cases where dyssynchrony is identified, implantable devices for synchronization and pacing, such as cardiac resynchronization therapy (CRT) devices, may be employed to improve the coordination of ventricular contractions and enhance overall cardiac function [5]. Thus, a thorough understanding of both the classification based on LVEF and the underlying etiology allows healthcare professionals to formulate personalized treatment strategies for heart failure patients. The treatment of HFpEF usually considers managing the underlying diseases behind it.

2.1.1 Cardiac Resynchronization Therapy (CRT)

Left ventricular (LV) dyssynchrony is a common pattern observed with HF and approximately one third of HF patients have left bundle branch block (LBBB) which causes electrical and mechanical delay between left and right ventricular contraction [39]–[41]. This impaired contraction decreases the efficiency of contraction and cardiac output [11]. Cardiac resynchronization therapy (CRT) is an established strategy that is based on implantable devices and used to deal with HF cases with impaired cardiac function during the last decades [5], [10], [11].

CRT devices are small devices that are connected to the heart with three wires and modify the impaired activation of ventricles, sense anomalies in contractions, and correct irregular patterns by radiating necessary electrical pulses [11], [12]. Reversal of heart irregularities provides efficient contraction and improvements in cardiac function [42].

The effectiveness of CRT on different patient groups has been evaluated in different clinical trials [43]–[46]. In these trials, the majority of HF patients have experienced significant recovery and reverse modeling. However, approximately one-third of patients could not utilize the CRT and achieve a positive response [47].

The CRT management process encompasses a crucial follow-up stage designed to identify factors predicting positive clinical outcomes and develop approaches for

addressing non-responders. This includes selecting suitable patients, implementing effective implantation strategies, and optimizing therapy benefits through programming. However, there is a lack of consensus about the prevalence of non-response and treatment strategies for CRT non-responders.

In assessing CRT response, various measures are utilized, including volumetric changes of the left ventricle, quality of life (QOL) assessments, and functional capacity evaluations [17]–[19]. Clinical trials and real-world practices often use different criteria to evaluate responses, with trials emphasizing event-driven endpoints like heart failure hospitalizations and mortality, while real-life situations prioritize the overall well-being of patients [17]. Event-driven endpoints such as heart failure hospitalization are crucial in large-scale trials [13], [48], but may not be as meaningful in individual clinical practice [17].

2.2 Mechanocardiography (MCG)

Seismocardiography (SCG) is a method that uses accelerometers placed on the chest to track the linear acceleration sourced by cardiac vibrations, whereas gyrocardiography (GCG) refers to the use of gyroscopes to track angular acceleration [21], [23]. Mechanocardiography (MCG) is a joint concept that includes both SCG and GCG to acquire a 6-axis representation of the mechanical activity on sternum with combining mutually orthogonal signal sources [24], [49]. The acquired vibrations thorough these sensors are sourced by contraction of the heart muscles, activies of heart valves, and the ejection of the blood and it is shown that these vibrations comprises information about hemodynamic variables, timing of different cardiac events, physiological and pathological state of heart in various different aspects [23], [26], [28], [50], [51]. An example for SCG waveform is represented in Figure 2.1.

In the literature, the waveform annotations on SCG and GCG signals are studied through simultaneous recordings of these modalities with echocardiography and

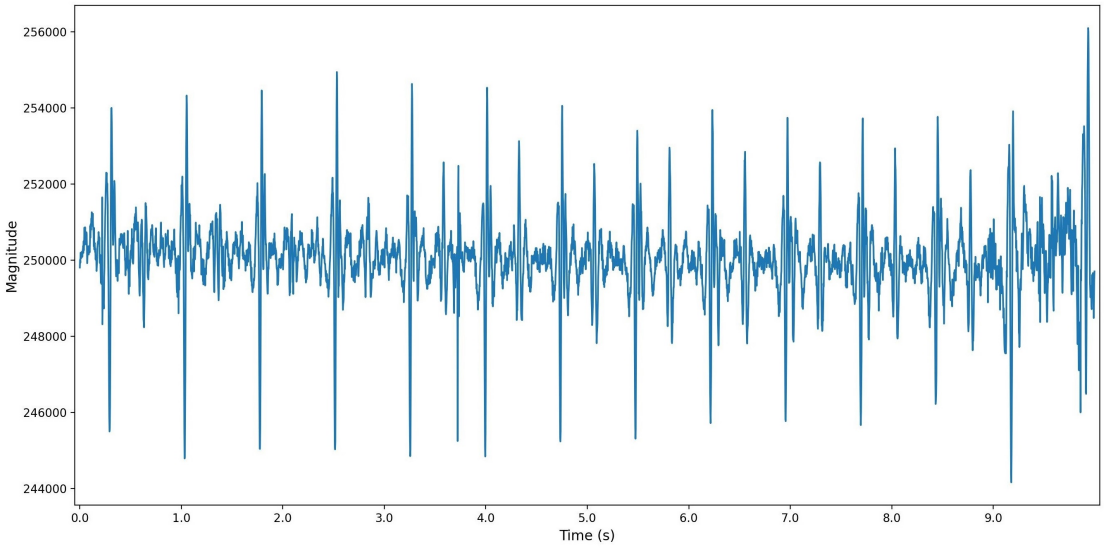

Figure 2.1: Example SCG signal from MECHANO-HF database (Z axis).

electrocardiography. Studies inferred that SCG and MCG show special correlations with intra-cardiac events and annotated the fiducial points that refer to mitral valve opening (MO) and closure (MC), aortic valve opening (AO) and closure (AC), rapid ejection (RE), and isovolumetric contraction (IVC) [20], [23], [52]–[55]. Annotation of these points enabled the inference for timing of cardiac event and further analysis of hemodynamics. Left ventricular ejection time (LVET), pre-ejection period (PEP), isovolumetric contraction time (IVCT) and isovolumetric relaxation time (IVRT) are some timing properties derived from SCG and GCG in the literature [23], [54], [56], [57]. These cardiac time intervals are important clinical markers for the analysis of systolic and diastolic function and therefore the detection of cardiac abnormalities [58], [59].

In addition to cardiac time intervals, fiducial points provide an opportunity to analyze the morphological changes in MCG focusing on the cardiac phase/intracardiac event of interest. Smaller analysis windows focused on different fiducial points have been used in the literature for representation of systolic and diastolic features separately. Some of the common features in the morphologic analysis are kinetic

energy, vertical range, i.e. difference between maximum amplitude and minimum amplitude, mean, median, and maximum amplitude in a selected window. The correlation between these features and cardiac contractility was analyzed in different settings [26], [29], [60].

MCG signals are affected by different additional sources like motion artifacts, environmental effects and sensor interference, and this source of artifacts can lead to errors in the feature calculation and further analysis [61], [62]. Thus, automatic annotation of fiducial points and temporal analysis requires a well-designed preprocessing pipeline. In the literature, the SCG components below 1 Hz were found to be correlated with respiration-related movements, while components between 1-20 Hz and above 20 Hz were correlated with vibrational and acoustic effects resulted from cardiac activity, respectively [63]–[65]. Also, it has been indicated that S1 and S2 heart sounds occur between 50 and 500 Hz, and S3 sounds lie at lower frequencies, between 20 and 200 Hz [66]. The available information regarding different frequency components can be used in the design of the preprocessing pipeline according to the interested characteristics and activity in the MCG signals.

2.3 Electrocardiogram (ECG)

The electrocardiogram (ECG) is a diagnostic method that displays changes in the bio-electrical activity of the heart over time [12]. It involves a non-invasive measurement technique, which includes placing electrodes on the patient's skin to capture electrical impulses [67]. Depolarization and repolarization events that occur in the heart chambers manifest with distinct morphologies over time, and the visual assessment of these events is crucial for evaluating and diagnosing cardiac conditions [68]. In clinical settings, ECGs are crucial for the detection of myocardial infarction, cardiac ischemia, heart failure, arrhythmias, and a wide range of cardiac conditions and diseases [69], [70].

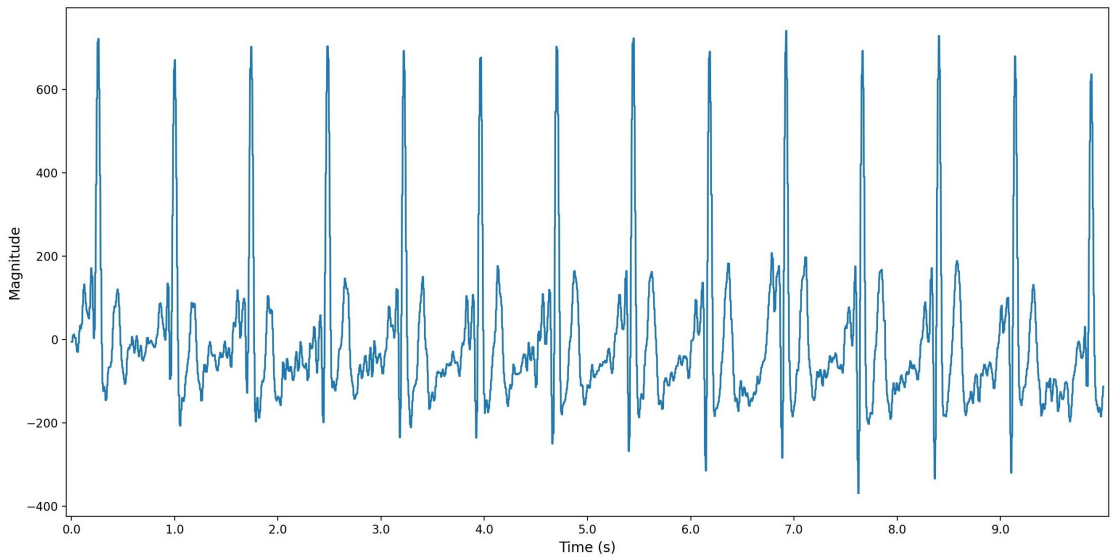

Figure 2.2: Example ECG signal from MECHANO-HF database.

ECG signals are utilized by visually evaluating the important morphological structures they contain in a clinical setting. Electrical activity in the heart muscles generates the PQRST morphology in ECG recordings (Figure 2.2). The P wave occurs with the initiation of an electrical impulse in the atria, signifying atrial depolarization and contraction. It is followed by the QRS complex, which indicates ventricular depolarization, leading to ventricular contraction. The T wave represents ventricular repolarization, showing the recovery phase when the electrical balance returns to its initial state [68]. Evaluating these waveforms can help clinicians extract information about the rhythmic, structural, and inflammatory aspects of the heart's condition [70].

ECG signals are also employed to extract significant time points in heart activity, supporting diverse analysis pipelines. The R peaks in ECG recordings are extensively used in biomedical signal processing applications to segment the signals coming from different sources into individual heartbeats [55]. In addition, R peaks are utilized to measure pulse transition time (PTT) in photoplethysmography applications [71]. The detection and analysis of Q waves are also essential, as they show

the initiation of ventricular systole and are used to calculate QS2 (electromechanical systole) duration. Various methods for automatically detecting PQRST waveforms are proposed in the literature [72]–[74].

2.4 Statistical Hypothesis Testing

Statistical hypothesis testing is a fundamental method employed in research and data analysis to assess the validity of a hypothesis. In this process, researchers formulate two hypotheses: the null hypothesis (H0) and the alternative hypothesis (H1). The null hypothesis represents the default assumption and often states the absence of an effect or no difference, while the alternative hypothesis defines the desired outcome or the presence of a specific effect. The aim is to determine if there is enough evidence in the sample data to reject the null hypothesis in favor of the alternative hypothesis. To make this decision, a p-value is calculated using various statistical formulas tailored to the specific characteristics of the sample data. The p-value is then compared to a predetermined significance level (α), usually set at 0.05, to determine statistical significance. If the p-value is less than or equal to α, the null hypothesis is rejected; otherwise, it is accepted [75], [76]. Statistical tests can be broadly categorized into two groups based on the assumptions they rely on: parametric tests and non-parametric tests.

2.4.1 Parametric Tests

Parametric tests are based on the assumption that the given data follows a specific probability distribution, typically the normal distribution. This assumed distribution is employed in the calculation of data statistics, such as mean and variance, and, consequently, the test's power and precision depend on the accuracy of this assumption. It is important to note that a violation of the assumption of normality

can effect the validity of parametric tests, and in cases where the data deviates significantly from a normal distribution, alternative non-parametric tests may be more appropriate. Common examples of parametric tests include the t-test and linear regression [77], [78].

2.4.2 Nonparametric Tests

Nonparametric tests (distribution-free tests) utilize less or no assumption about the distribution of data. They are used on data that does not meet the assumptions emerging during the use of parametric tests or has ordinal characteristics. In such situations, nonparametric tests provide reliable and valid results.

Another key feature of nonparametric tests is their ease of application to small sample sizes, where parametric tests might be less reliable. This makes them valuable in situations where limited data is available or when strict experimental conditions restrict the sample size. Furthermore, nonparametric tests are less sensitive to the shape of the distribution and, therefore, more robust in scenarios where the underlying data distribution is unknown. For this reason, they are valuable and robust, even though they may have less statistical power compared to parametric tests. Some examples of non-parametric tests are the Mann-Whitney U test, the Wilcoxon signed-rank test, and the Kruskal-Wallis test [79]–[81].

Wilcoxon Signed-Rank Test

The Wilcoxon signed-rank test is a non-parametric statistical test used to determine whether the distribution of differences between paired samples is symmetric about a specified median and assess whether there is a significant shift in the distribution of differences [80]. This test is particularly useful when analyzing paired data, when each pair of observations is related in some way (e.g., before-and-after measurements or control-treatment pairs), parametric assumptions are not met, or data does not

follow a normal distribution.

The test involves ranking the absolute differences between each pair of observations, considering their signs, and then summing the ranks of the differences. The test statistics formula for Wilcoxon signed-rank test is $W = \sum_{i=1}^{N_r}[sgn(x_{2,i} - x_{1,i} \cdot R_i))]$ where W is the test statistic, N_r is the sample size, sgn is the sign function, $x_{2,i}, x_{1,i}$ are corresponding pairs from two distributions, and R_i is the rank.

3 Related Work

3.1 Filtering of MCG Signals

Filtering of the MCG signals is fundamental for the analysis and interpretation of the cardiac vibrations. In this chapter, we introduce different filtering methodologies applied to MCG signals in the literature.

3.1.1 Frequency Filters

Frequency filters play a crucial role in altering the content of signals in electronics and signal processing. Low-pass filters allow lower frequencies to pass through while reducing higher ones, making them useful for eliminating noise or focusing on fundamental signal elements. High-pass filters, in contrast, allow higher frequencies to pass while diminishing lower ones, finding application in situations where low-frequency elements are undesirable. Band-pass filters are designed to enable a specific range of frequencies to pass through, excluding those outside the designated band. These filters are useful for isolating desired frequency components. Band-stop filters, on the other hand, target and reduce a narrow band of frequencies, useful for removing interference or specific unwanted components [82].

Butterworth, Chebyshev, and elliptic (Cauer) filters are among the most popular types of filters, each offering distinct advantages. The Butterworth filter provides a maximally flat frequency response in the passband, making it suitable for applica-

tions where a consistent gain across frequencies is crucial. Chebyshev filters, on the other hand, allow for a steeper roll-off at the expense of some ripple in either the passband (Chebyshev Type I) or the stopband (Chebyshev Type II). This flexibility makes them ideal for scenarios where a sharper transition between the passband and stopband is required. Elliptic filters offer the steepest roll-off among these filters.

In MCG, filtering methodology and the selected passband depend on the specific research or diagnostic goals. In seismocardiogram analysis, components below 1 Hz are associated with respiration-related movements, those between 1-20 Hz and above 20 Hz are linked to vibrational and acoustic effects from cardiac activity, and specific heart sounds such as S1 and S2 occur between 50-500 Hz, while S3 sounds lie in lower frequencies between 20-200 Hz [63]–[66]. Based on the desired component to analyze, different frequency filters can be designed with the corresponding frequency range and properties. For instance, in [32], it is proposed that most information regarding cardiac vibration exists above 1 Hz and a bandpass filter with a pass band of 1-45 Hz was used. In [23], a 4th-order Butterworth filter with passbands of 1–20 Hz and 4–45 Hz were used for GCG and SCG, respectively. In [55], a 0.05 Hz highpass and 90 Hz lowpass filter were used for extracting the mean heartbeat and analyzing SCG morphology, while a 50–500 Hz bandpass filter was used in the same study for analyzing heart sounds. For focusing on the mean heart beat morphology, the baseline and frequency components higher than 90 Hz were eliminated. However, heart sounds occur in the higher components so that the high-frequency components were preserved for heart sound analysis.

Moreover, different filtering options can be used in the same analysis pipeline to reveal the effects of different SCG components. In [62], six different filtering options (0-1 Hz, 0-20 Hz, 0-40 Hz, 1-20 Hz, 1-40 Hz, 20-40 Hz) on SCG signals were used and machine learning models were trained for the prediction of the metabolic equivalent of task (MET) scores using one of the defined filtering options. Analyzing the model

performances, the informativeness of different SCG components in the estimation was discussed and it is found that respiration-related SCG components are critical for MET estimation.

3.1.2 Wavelet Transform Approach

Wavelet transform is a technique employed in signal and image processing for various purposes such as denoising, compression, and feature extraction [83]–[85]. Utilizing small basis functions known as wavelet, the wavelet transform decomposes the signal into representations that shows different frequency components at different resolutions [84], [86]. This transformative approach is advantageous, especially in heart sound detection, as it allows a focused examination of distinct frequency components, thereby enhancing the clarity of heart sounds while mitigating the impact of high-pitched noises in MCG signals [87]. Earliest studies [88] applied wavelet transform to phonocardiogram signals, and the literature presents diverse methods for leveraging wavelet transform in fiducial point detection and heart sound extraction on SCG signals [89]–[91].

The primary application of wavelet transform involves extracting different detail and approximation waveforms of the MCG signals at various levels and utilizing these waveforms. The signal processing pipeline preceding and following the wavelet decomposition stage varies across different studies. Additionally, the wavelet decomposition step may differ based on the choice of the mother wavelet used in the decomposition process. In the literature, Morlet wavelet and Daubechies wavelet families were mostly utilized and proposed as the mother wavelets for especially heart sound analysis [92]–[95].

3.1.3 Synchronized Averaging Approach

Synchronized averaging is a signal processing technique designed to enhance the clarity of cardiac vibrations observed in MCG measurements. Synchronized averaging includes the synchronization of heart beats with the detected reference points and the averaging of MCG signals over multiple cardiac cycles [64], [65]. One primary benefit is noise reduction, since the technique reduces the impact of random noise and motion artifacts in recordings. By highlighting consistent components across multiple cycles, synchronized averaging increases the signal-to-noise ratio and provides a cleaner representation of the cardiac vibrations.

3.2 Fiducial Point Detection on MCG Signals

Various cardiac events lead to distinct waveform morphologies at different MCG axes. Detecting the time points of these cardiac events helps in analyzing the specific cardiac event and identifying various timing features applicable to cardiac health assessment. Despite fiducial points being annotated on SCG and GCG signals in the literature, and approximate morphologies around these events being known, the presence of noise due to motion artifacts, deviations caused by respiration, or intersubject variability resulting from body mass distribution, gender, and age differences may create differences in these morphologies [32], [96], [97]. Therefore, detecting fiducial points can be challenging and prone to errors. Various approaches are proposed in the literature to facilitate the identification of fiducial points on MCG signals.

3.2.1 Search Windows

This approach is grounded in restricting the search area where the detection algorithm operates. The cardiac time intervals for various events are already docu-

mented in the literature for both healthy subjects and those with different cardiac conditions [98]–[101]. These timings can be leveraged during the search for fiducial points, allowing the search to focus solely on the signal segment known to contain the fiducial point of interest. This method helps eliminate misleading and similar morphologies occurring in the heartbeat, ensuring that the detected point is within the corresponding search window. Once the search window is defined, the detection algorithm specific to the interested morphology can be executed only for the segment within the search window. However, it is important to note that this method necessitates reference points to delineate the search window.

For example, in [102], a 90 ms search window was established to identify aortic valve opening points on SCG signals, based on the detected R-peaks on the ECG signals. In [103], AO on SCG was determined as the maxima occurring after 45 ms and before 125 ms following the detected Q wave in the ECG. For aortic valve closing (AC), AO was utilized as a reference and AC was defined as the maxima within the interval [AO + 240 ms, AO + 350 ms]. Similarly, in [104], a 250-ms-long search window was employed starting from 200 ms after S1 and S2 was defined as the minimum wave in the search window.

3.2.2 Dynamic Time Warping

Dynamic Time Warping (DTW) is a dynamic programming-based algorithm used to align two sequences that may have different lengths [105]. The aim is to find an optimal alignment between the samples of the sequences that matches one sample from the first sequence to the other. This matching may not be necessarily one-to-one due to the possible length differences between sequences. The dynamic programming is utilized to minimize the pre-defined distance metric that qualifies the quality of alignment, and the algorithm aims to find optimal alignment between these sequences based on specified constraints. These constraints may include monotonicity, conti-

nuity, boundary, warping window, and slope [106], [107]. DTW is generally used for aligning sequences that are morphologically similar but occur at different paces, e.g., speech recordings contain identical content but are pronounced at different paces.

DTW includes the construction of a cost matrix that includes the cost of alignment for each possible sample pair [105]. Dynamic programming recursively finds a warping path that minimizes the total cost and aligns the sequences according to the constraints. The cost function may be simply defined as the Euclidean distance of samples; however, new cost functions can be defined and utilized [108]–[110].

In [111], DTW was applied for fiducial point detection on SCG signals. They utilized an intermediary reference signal pair consisting of ECG and SCG signals with a specific RR interval. They proposed a hybrid cost function for DTW that considers differences in signal values, neighborhood shifting level, signal slope, and concavity and provided a flexible and adaptable approach for accurate fiducial point detection. The fiducial point, such as the aortic valve closing event, is detected in the reference SCG signal and then projected to the nonreference SCG signal using DTW-based quasi-synchronous alignment.

3.2.3 Hidden Markov Model

A Hidden Markov Model (HMM) is a statistical model used to represent an evolving system whose state is not directly observable but can be inferred from observed data. It consists of a set of hidden states, observable outputs, and transition probabilities between states. The probability of observable outputs depends on the underlying state chain, and based on observable outputs, the underlying state transition probabilities can be estimated [112].

In the literature, the HMM method is applied to seismocardiogram signals to estimate heart rate, heart rate variability, and cardiac time intervals [113]. In [113], SCG heartbeats were defined with N hidden states and modeled a sequential tran-

sition between states. The value of N was determined based on the heart rate of the corresponding subject. Following the modeling, they employed the Baum-Welch algorithm to estimate the parameters of the defined statistical model and identified the state of each sampling instance. For detecting cardiac events, they utilized one manual annotation of the cardiac events for each subject and labeled the states corresponding to the fiducial points. Using the time points of the same states in the subsequent cycles, they detected the fiducial points of the following cycles and measured cardiac time intervals.

3.3 Assessment of Cardiac Function with MCG Signals

3.3.1 Cardiac Performance

To analyze and measure changes in cardiac function using MCG signals, understanding the correlation between the time and frequency domain properties of MCG and underlying physiological variables is crucial. Various time and frequency domain features have been generated and analyzed in the literature concerning the known pathological effects of different diseases. To acquire information about the overall trend of magnitude, certain features are defined:

- **Amplitude:** $A = x(t)$ [29], [60].
- **Maximum Amplitude:** $A_{\max} = \max_t x(t)$ [114], [115].
- **Minimum Amplitude:** $A_{\min} = \min_t x(t)$ [114].
- **Vertical Range:** $R = \max_t x(t) - \min_t x(t)$ [29], [114].
- **Power:** $P = \sum_{t=1}^{N} x(t)^2$ [115].

- **Root Mean Square Power:** $P_{\text{rms}} = \sqrt{\frac{1}{N}\sum_{i=1}^{N} x_i^2}$ [24], [60], [114], [115].
- **Linear Kinetic Energy:** $K_{\text{Lin}}(t) = \frac{1}{2}m(v_x^2(t) + v_y^2(t) + v_z^2(t))$ where $v_x(t)$, $v_y(t)$, and $v_z(t)$ are the velocities in the x, y, and z directions, respectively [26].
- **Rotational Kinetic Energy:** $K_{\text{Rot}}(t) = \frac{1}{2}(I_{xx}\omega_x^2(t) + I_{yy}\omega_y^2(t) + I_{zz}\omega_{zz}^2(t))$ where I_{xx}, I_{yy}, and I_{zz} are the moments of inertia and $\omega_x(t)$, $\omega_y(t)$, and $\omega_{zz}(t)$ are the angular velocities in the x, y, and z directions, respectively [26].

These features are associated with the cardiac performance of the heart in different studies. For instance, in [26], it is found that kinetic energy calculated from MCG measurements is related to cardiac contractility. Similarly, in [29], an increase in the vertical range was reported when the pacemaker was turned on, indicating better left ventricular function. In [116], a relationship between left ventricular contractility and the maximum magnitudes acquired from an accelerometer sensor placed on the chest of minipigs was proposed. In line with these findings, the magnitudes observed in MCG measurements can be related to the strength of heart contraction, reflecting the performance of cardiac function.

3.3.2 Cardiac Time Intervals

Cardiac time intervals are crucial parameters for assessing heart function and diagnosing cardiovascular disorders. These intervals include left ventricular ejection time (LVET), pre-ejection period (PEP), and total electromechanical systole period (QS2). After detecting fiducial points on MCG and ECG signals, these cardiac time intervals can be measured by calculating the time difference between the fiducial points of interest. In the literature, these time intervals were derived from MCG signals and defined as follows:

- **PEP:** Time difference between the Q wave and AO [28], [117].

- **LVET:** Time difference between AO and AC points [28], [54], [56], [57], [118].
- **QS2:** Time difference between the Q wave and AC [118].

In the literature, variations in LVET have been proposed to be associated with conditions such as heart failure [99], [119], [120], hypertension [121], and ischaemic heart disease [122]. The PEP could serve as an indicator of increased sympathetic nervous system activity or impaired ventricular contractility [123], [124], while abnormalities in the QS2 may suggest an increased risk of mortality, particularly in cases of coronary artery disease [125]. Therefore, these time intervals are crucial and important as they allow us to analyze the cardiac health of patients.

4 MECHANO-HF Dataset

MECHANO-HF dataset was collected at Turku University Hospital (TYKS) and it contains data from 10 CRT patients. All patients were diagnosed as HFrEF and had previously obtained a CRT pacemaker. Inclusion criteria required participants to be

- at least 18 years old
- capable of understanding and consenting by signing an informed consent form
- in stable clinical condition without significant valve disease, rhythm irregularities, or significant clinical instability.

Variable		
Age (year)	Mean (±SD)	73.98 (±7.52)
Sex	Males, n	8
	Females, n	2
Height (cm)	Mean (±SD)	172.20 (±6.97)
Weight (kg)	Mean (±SD)	92.80 (±22.95)
BMI (kg/m²)	Mean (±SD)	31.00 (±5.59)
Left ventricular ejection fraction (%)*	Mean (±SD)	39.90 (±8.77)
NYHA class	I, n	1
	II, n	4
	III, n	4
	IV, n	1

Table 4.1: Baseline characteristics of patients included in the study. (*After introduction of optimal medical treatment and CRT)

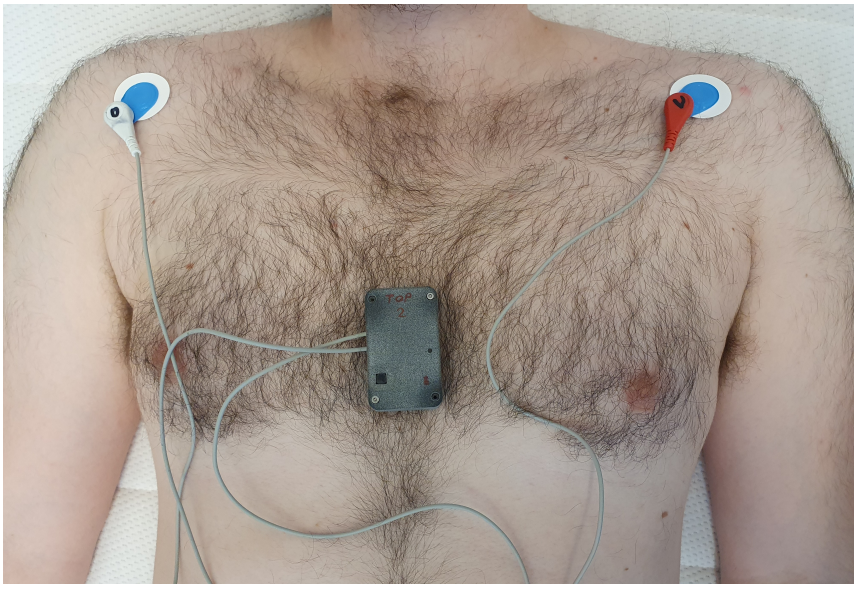

Figure 4.1: The device is positioned on the lower part of the patient's chest, recording 3-axis acceleration, 3-axis rotation, and a single-lead ECG while the patient is in a supine position. This illustration has been adapted from the original figure featured in the article [24] under the license CC-BY 4.0.

The study's baseline demographics are detailed in Table 4.1, and ethics approval was obtained from the Ethics Committee of the Hospital District of Southwest Finland, aligning with the 2002 Declaration of Helsinki. All participants provided written informed consent.

A custom-designed device, incorporating a 3-axis accelerometer (ADXL355, Analog Devices Inc., Wilmington, MA, USA), a 3-axis gyroscope (LSM6DS3, STMicroelectronics, Geneva, Switzerland), and a single-lead ECG, was used for data collection. The device had accelerometer and gyroscope measurement ranges of ±2 g and ±250 dps, respectively. The accelerometer's noise density was $25\mu g/\sqrt{Hz}$, and the gyroscope's rate noise density was $7mdps/\sqrt{Hz}$. The sensor was placed on the lower chest (Figure 4.1). Each measurement included signals from one accelerometer and one gyroscope for each of the three axes, along with a single-lead ECG. Simultaneous recording of MCG and ECG was conducted.

Recordings took place with patients in a supine position after a 15-minute rest

in a quiet environment. Patients were instructed to breathe normally, avoid talking, and minimize unnecessary movements. The pacemaker was randomly set to AAI or CRT mode, with a heart rate of 80 bpm to maintain a consistent heart rate throughout measurements. In AAI mode, only the atrium is paced, resulting in dyssynchronous ventricular function, while the optimized CRT mode aims to resynchronize ventricular contraction.

5 Proposed Method

5.1 Signal Processing

Respiratory-related variations and baseline measurements are evident in the lower frequency components of the MCG signal, potentially causing significant fluctuations [126]. Conversely, high-frequency components can introduce ambiguity in the fiducial point detection process, even though their impact on the waveform is less pronounced than that of low-frequency artifacts. To enhance the analysis of cardiac activity, signal processing plays a crucial role in MCG analysis. In this section, we introduce our signal processing pipeline.

5.1.1 Signal Resampling

The dataset contains ECG and MCG measurements recorded simultaneously for a duration ranging from 8 minutes to 12 minutes. Before further processing, ECG and MCG signals of the corresponding measurement were synchronized and resampled to 400 Hz.

5.1.2 Noise Removal

Initially, segments with high motion interference and low signal quality were manually excluded. Thirty-second-long segments were chosen from each MCG measurement for analysis. Subsequently, a forward-backward filtering operation was applied

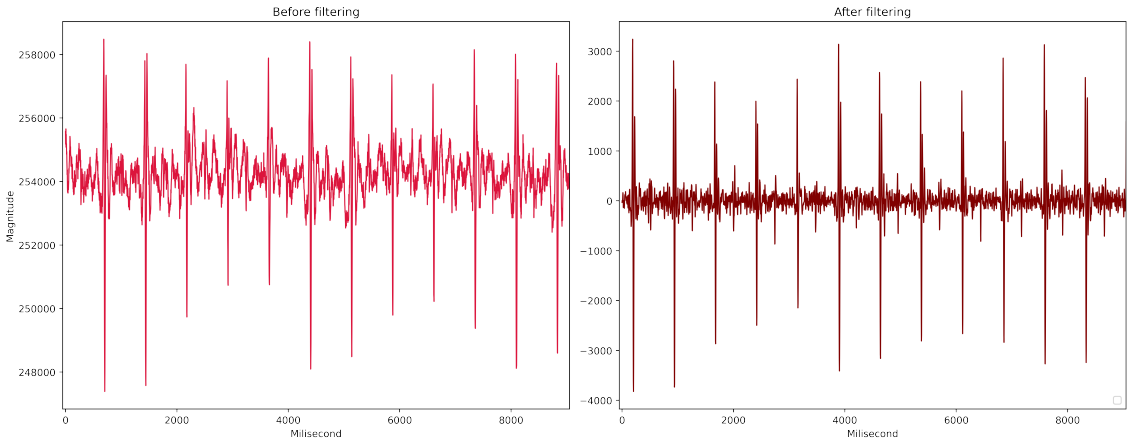

Figure 5.1: Example SCG-Z signal from MECHANO-HF database before filtering (left) and after filtering (right).

to SCG-Z signals. A Butterworth bandpass filter with a 20-90 Hz passband was selected for its desirable characteristics, which include a maximally flat frequency response within the passband and a smooth roll-off. The application of this filter aids in refining the MCG waveform. Figure 5.1 illustrates the SCG-Z signal both before and after the application of the filtering process. Finally, the 30-second segments were further divided into 10-second segments for the rest of the analysis.

5.1.3 R Peak and Q Wave Detection

Hamilton's algorithm, as outlined in [72], was utilized for R-peak detection in ECG signals. The process involves preprocessing to reduce noise, the application of a band-pass filter to isolate the QRS complex, and the use of techniques such as differentiation and squaring to identify and enhance the R-peaks. The algorithm establishes a threshold to select peaks above a certain height, providing accurate timing for when the heart's ventricles depolarize in ECG readings. Additionally, the detection of Q waves in the ECG signals was performed using the wavelet-based delineation algorithm available in the NeuroKit2 toolbox [127]. Example ECG recordings with annotated R peaks and Q waves are represented in Figure 5.2.

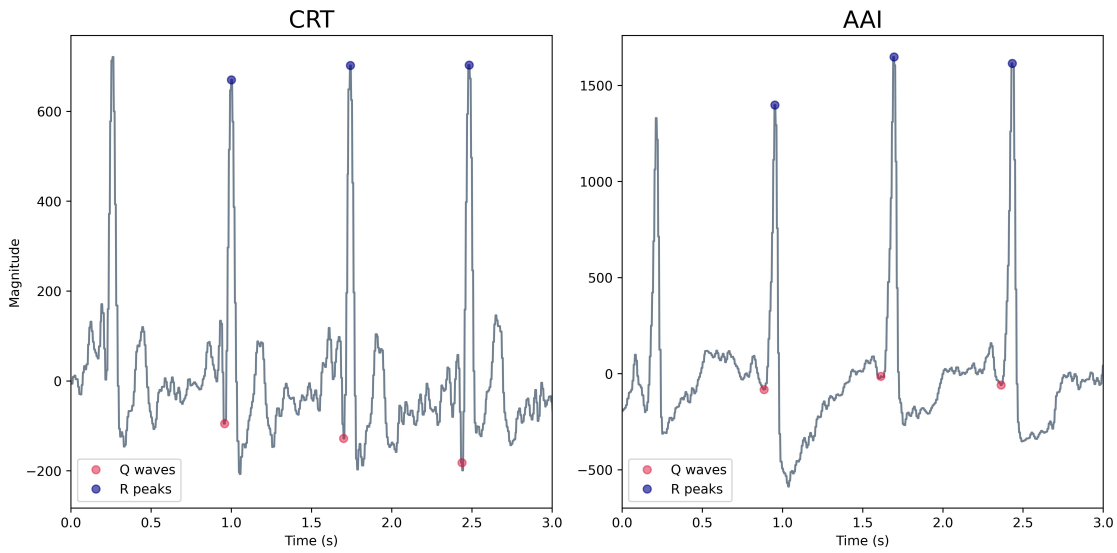

Figure 5.2: Example ECG signal with detected Q waves and R peaks in a heart failure patient undergoing CRT pacing (left panel) and AAI pacing mode (right panel).

5.1.4 Aortic Valve Opening & Closing Detection

Following the detection of R-peaks, each individual heartbeat has been successfully identified. To annotate the aortic valve opening (AO) and aortic valve closing (AC) points, a search window approach was employed. For each heartbeat, the aortic valve opening point was determined as the maximum peak point of the SCG-Z axis within the first 125-ms interval after the corresponding R peak.

The left ventricular ejection time (LVET) represents the duration between the opening and closing of the aortic valve during each cardiac cycle. The search window for aortic valve closing (AC) was defined based on reported LVET and left ventricular ejection time index (LVETI) in the literature [99], [128], utilizing the detected AO points as reference.

Consequently, a 60-ms long window was positioned 240 ms after the corresponding AO, and AC was identified as the maximum peak within the interval between 240-300 ms after the AO. AO and AC detection operations were exclusively con-

ducted on the SCG-Z signals, with the same locations employed on other axes from the same segment and synchronized with the same reference as the corresponding SCG-Z signal.

5.1.5 Filtering

Various frequency components in the MCG measurements were suggested to be linked to different sources of information. Specifically, SCG components between 1 and 20 Hz are associated with mechanical vibrations, while those above 20 Hz are linked to acoustic effects caused by cardiac activity [64], [65]. To analyze the effect of CRT on these components separately, we designed four distinct first-order Butterworth filters with a passband chosen from the following options: 20-90 Hz, 6-90 Hz, 1-20 Hz, and >1 Hz (highpass). Each axis of the SCG and GCG in measurements was initially filtered with these specific filters and subsequently analyzed.

5.1.6 Vector Creation

To represent the total movement of the SCG and GCG sensors, SCG and GCG vectors were constructed. For SCG and GCG vectors, all three axes of the respective sensor were combined using the Euclidean formula. Furthermore, MCG vectors were created for each frequency range (>1 Hz, 20-90 Hz, 6-90 Hz, 1-20 Hz) by combining SCG and GCG vectors. However, as the GCG and SCG sensors have different measurement units and ranges, combining them required scaling these measurement units between [0,1] to ensure a comparable contribution from both sensors before their combination. To address this range issue, SCG and GCG vectors were scaled to fall within the [0,1] range. This scaling was achieved by utilizing the maximum and minimum values calculated for all vectors in the corresponding frequency ranges from the corresponding measurement units.

Firstly, all SCG and GCG vectors were extracted by filtering the signals with the

Listing 1 MCG Vector Creation

```
1: for frequency range in [> 1 Hz, 20-90 Hz, 6-90 Hz, 1-20 Hz] do
2:     for measurement unit in [SCG, GCG] do
3:         Create vectors
4:         Find the maximum and minimum value of all created vectors (1 max and
   min value for the whole set)
5:         Scale all vectors according to the maximum and minimum value
6:     end for
7:     Create MCG vectors
8: end for
```

selected pass band. Then, we identified the minimum and maximum values of the vectors coming from the sensors. All SCG and GCG vectors were scaled within [0,1] using the identified maximum and minimum values of the SCG and GCG vectors, respectively. The operation was applied each pass band option separately. The pseudocode for extraction of MCG vectors is presented in Listing 1.

5.1.7 Synchronized Averaging

For every signal in a 10-second segment, two mean heartbeats were generated. This process involved synchronized averaging using both the R peak and AO point as reference points. Synchronized averaging entails extracting individual heartbeats, aligning them based on their reference points, and averaging the heartbeats in relation to this alignment. Two examples for mean SCG vector beats are shown in Fig. 5.3. At the conclusion of this step, there were 72 average cycles for each 10-second segment, representing each of the 6 axes and 3 vectors (SCG, GCG, and MCG) filtered with the 4 filtering options, and 2 mean cycles for each.

5.2 Feature Extraction

In this section, we outline how features were generated from the processed MCG signals to support the comparison of waveform characteristics between CRT and

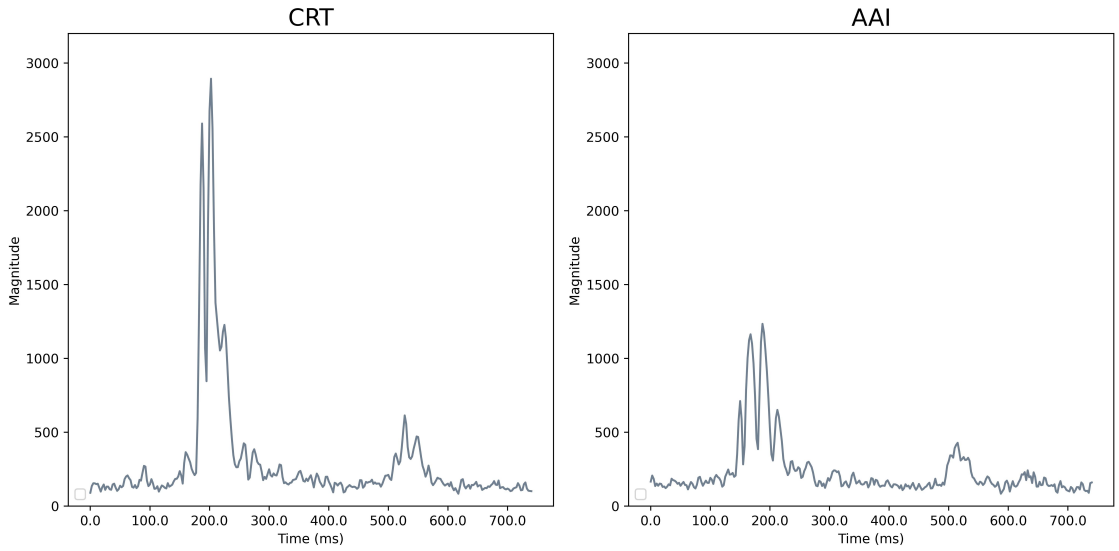

Figure 5.3: Example mean beat of SCG vector in a heart failure patient undergoing CRT pacing (left panel) and AAI pacing mode (right panel) based on AO averaging.

AAI modes.

5.2.1 Morphological Features

To extract features related to systolic and early diastolic characteristics, we initially identified the systolic and early diastolic regions in the signals by locating AO and AC points on SCG-Z averages. For each average cycle, two windows of 150 ms duration were created. One window centered on the detected AO, and the other window was placed immediately after AC to focus on the early diastolic region. These windows were termed systolic and early diastolic windows, respectively.

Subsequent to the creation of systolic and early diastolic windows, morphological features were extracted from these windows. These features included energy (E_x) and vertical range (R_x), and they were defined as follows:

$$E_x = \sum_{n=-\infty}^{\infty} x[n]^2$$

$$R_x = \max x[n] - \min x[n]$$

Example average cycles and extracted features are shown in Figure 5.4.

5.2.2 Timing Features

LVET and electromechanical systole (QS2) time intervals were also extracted as features. We determined the left ventricular ejection time (LVET) and electromechanical systole (QS2) by calculating the time duration between the identified AO and AC, and between the Q wave and AC, respectively.

5.3 Statistical Tests

Our goal was not only to identify potential differences between CRT and AAI modes but also to explore specific MCG components that exhibit the most significant distinctions, providing valuable insights into the optimal features for detecting differences. Accordingly, in the previous section, we extracted features from various mean cycles of MCG measurements differing in terms of frequency, axis, and synchronized averaging method. In this section, we will introduce the statistical analysis method that we employed in the study.

In our analyses into the differences between CRT and AAI modes in MCG waveforms, we conducted paired statistical tests on features extracted from various mean cycles. These cycles were obtained for all three 10-second segments that belong to the same measurements, allowing us to analyze distinct segments of the MCG recordings. Each experiment focused on one frequency component, axis, and synchronized averaging method combination and compared the corresponding MCG cycles in CRT and AAI modes.

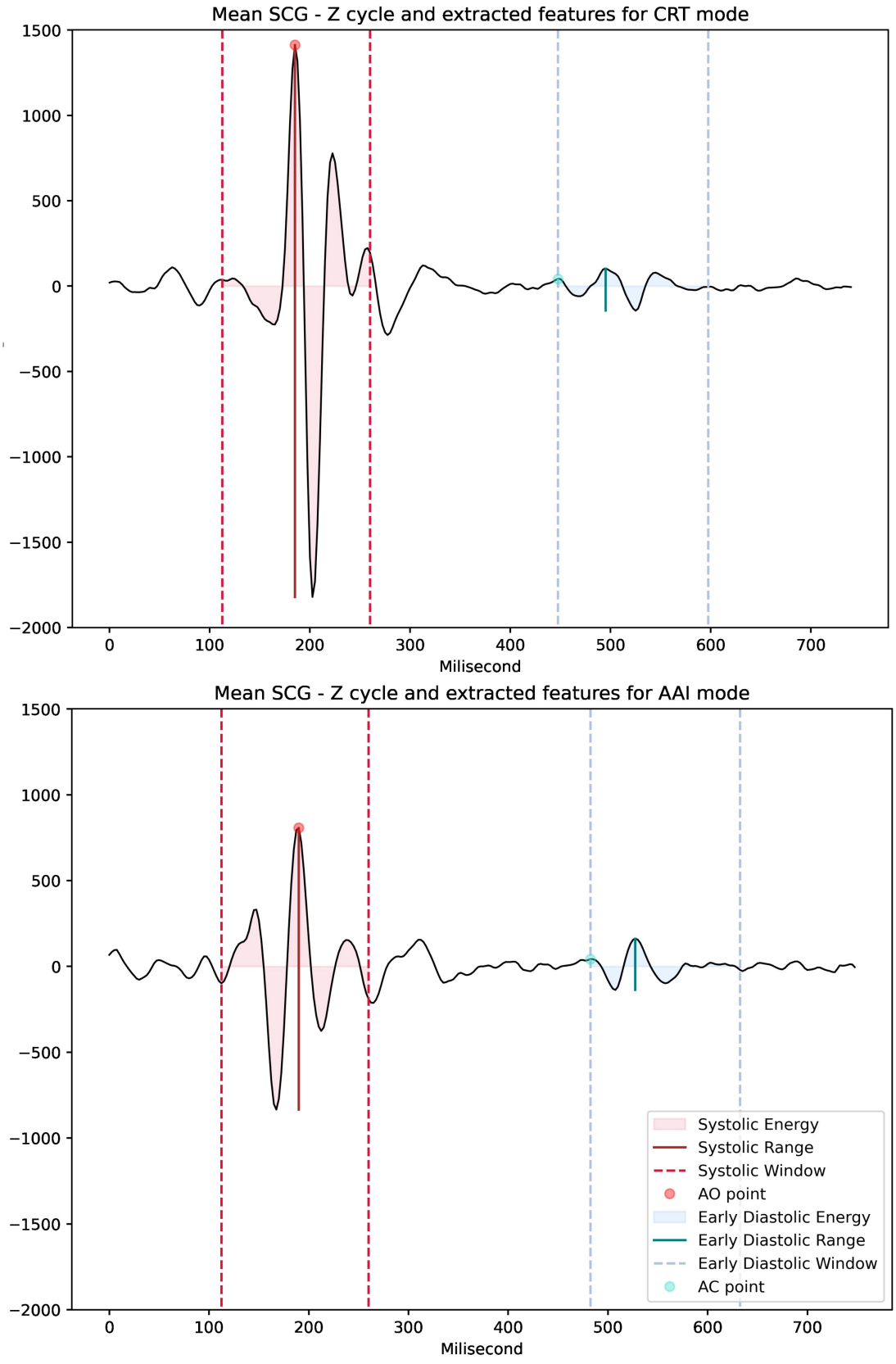

Figure 5.4: Definitions of extracted features in a heart failure patient undergoing CRT pacing (upper panel) and AAI pacing mode (lower panel) based on AO averaged SCG-Z cycle. This illustration has been altered from the original figure in the article [34] and is being utilized with explicit permission.

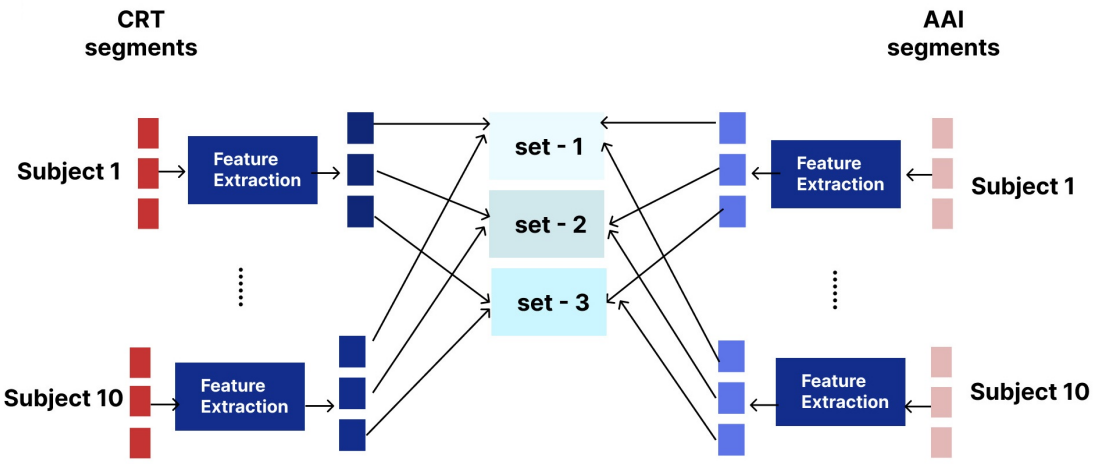

Figure 5.5: The distribution of segments to various sets involves putting the features of the first, second, and third segments of the corresponding mode into sets 1, 2, and 3, respectively, for each subject. The illustration presented here is a modified version of the original figure depicted in the article [34], used with permission.

The features from the first, second, and third segments were put into set-1, set-2, and set-3, respectively, creating three individual sets representing separate and non-overlapping parts of the recordings (Fig. 5.5). To enhance the robustness of our findings, we applied paired tests to each set, effectively creating a double-check mechanism and minimizing the risk of type I errors.

For each experiment, statistical comparisons were performed using the Wilcoxon signed-rank test, with a significance threshold of $p < 0.05$. We considered differences between pacing modes as significant only when the null hypothesis was rejected in all three paired tests conducted on set-1, set-2, and set-3. If any of the tests did not result in the rejection of the null hypothesis, we did not accept and report the alternative hypothesis, ensuring a rigorous evaluation of the observed differences between CRT and AAI modes (Fig. 5.6).

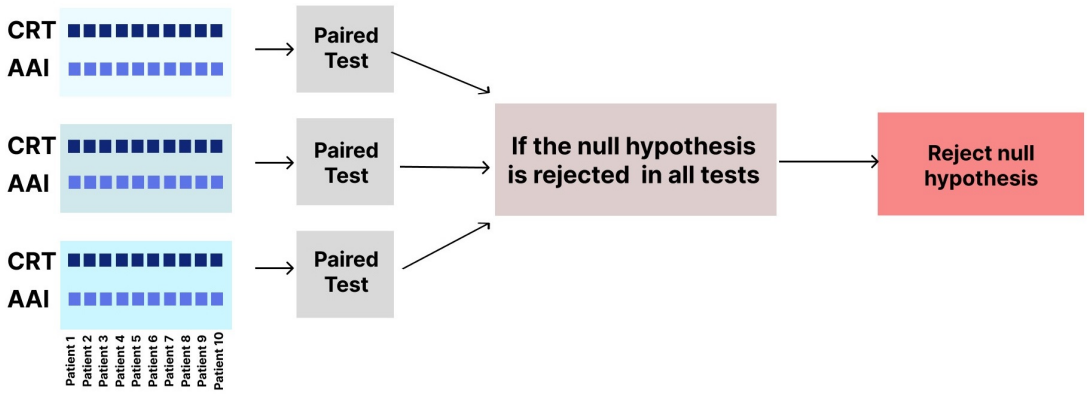

Figure 5.6: Algorithm for data analysis. Each individual paired set underwent a statistical test, and the null hypothesis was rejected if all parallel tests rejected the null hypothesis. The illustration shown here has been adjusted from the original figure in the article [34] and is being employed with permission.

6 Results

6.1 Morphological Features

In this chapter, we report the results of the statistical comparisons of morphological features extracted from measurements during CRT and AAI mode.

6.1.1 Systolic Features

Vertical range (R_x) and energy (E_x) in the systolic window exhibited statistical differences between the two pacing modes. During CRT pacing, systolic features were higher than those in AAI mode. The changes in systolic energy, vertical range for each axis, frequency range, and synchronization method were examined during the transition from CRT to AAI pacemaker mode and represented in Fig. 6.1. Statistically significant differences between the modes were denoted by colored squares. The percentage within the squares indicates the mean energy and vertical range change after initiating AAI pacing, relative to the values observed in CRT mode. The color gradients within each box illustrate the descending order of differences between all CRT-AAI segment pairs in the corresponding experimental settings.

Every SCG & GCG axis exhibited statistically significant differences in vertical range across at least one frequency range, resulting in $p<0.05$ for all three parallel statistical tests (Fig. 6.1). Additionally, SCG, GCG, and MCG vectors exhibited differences in systolic range between the two pacing modes. Differences were visible

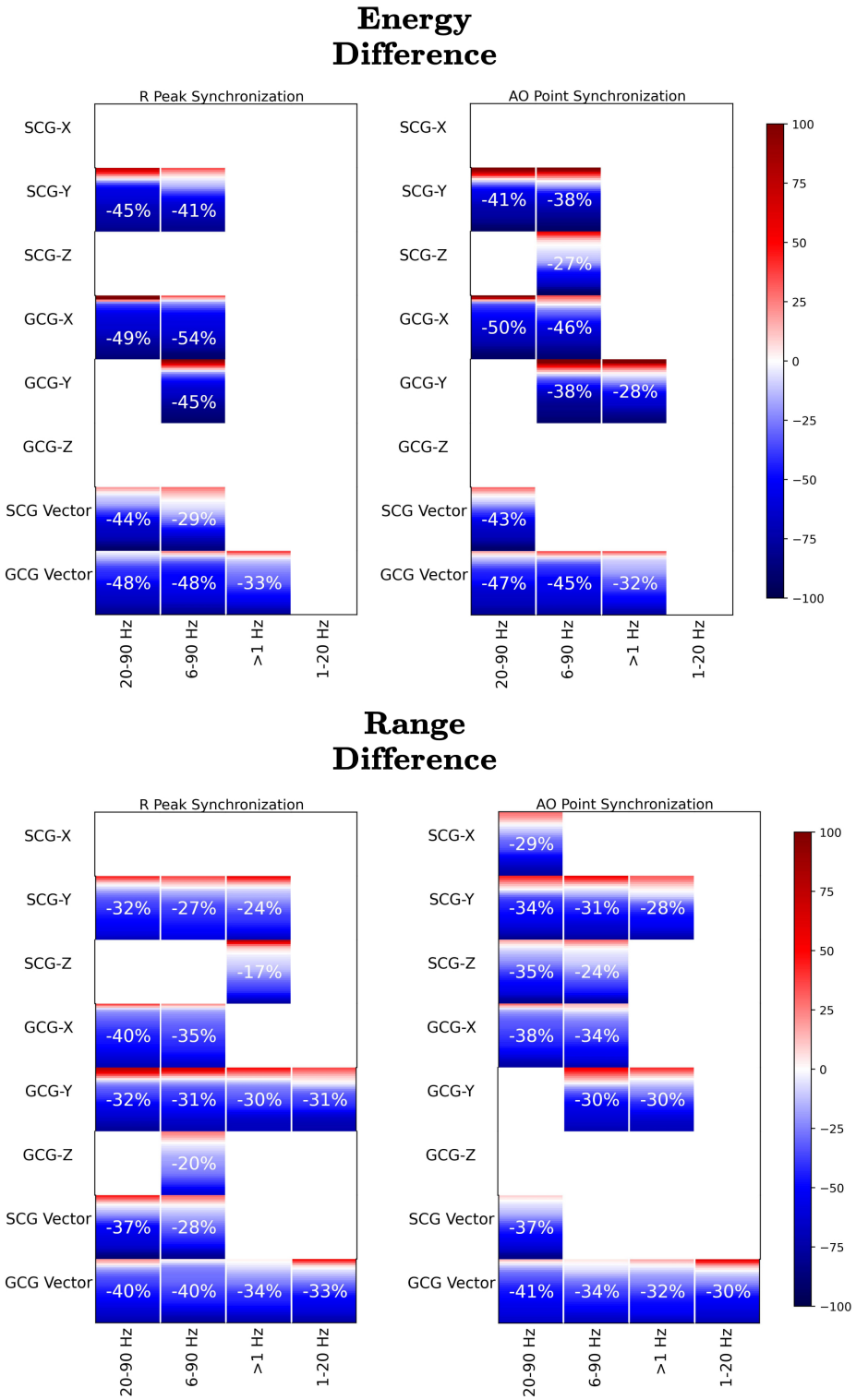

Figure 6.1: Changes in systolic energy and vertical range for each axis, filtering frequency and synchronization method. Adapted from the original figure featured in the article [34], this illustration has been modified and is utilized with permission.

	AAI : Mean (SD)	**CRT : Mean (SD)**	**Difference**
QS2	428 ms (± 35)	405 ms (± 46)	Not significant
LVET	273 ms (± 14)	269 ms (± 15)	Not significant

Table 6.1: Mean and standard deviation of QS2 and LVET during CRT and AAI mode.

in all frequency components, with the most noticeable changes occurring within the 6-90 Hz frequency range, remaining significant with the extension of the frequency range. AO Point and R peak synchronization yielded comparable results and showed differences in a slightly different experiment set. However, significant differences in the systolic range of the GCG-Z axis were observed in R-peak synchronization, while the difference in SCG-X was noteworthy only when synchronized with the AO point.

The increase in systolic energy when pacing mode changed from AAI to CRT was significant in the SCG-Y, SCG-Z, GCG-X, and GCG-Y axes, as well as in the SCG, GCG, and MCG vectors. Differences in systolic energy were more concordant in the GCG axes and GCG vector. Moreover, observable differences in systolic energy were present in the ranges that included higher frequency components, with the difference not being significant in 1–20 Hz. Systolic energy and vertical range changes in the GCG-X axis for each subject are shown in Figure 6.2.

6.1.2 Early Diastolic Features

Despite the differences found in systolic features, there were no significant differences observed in early diastolic features.

6.2 Timing Features

Table 6.1 presents the mean and standard deviation concerning measured QS2 and LVET during CRT and AAI pacing modes. The analysis revealed no notable differences in QS2 and LVET when comparing CRT and AAI modes.

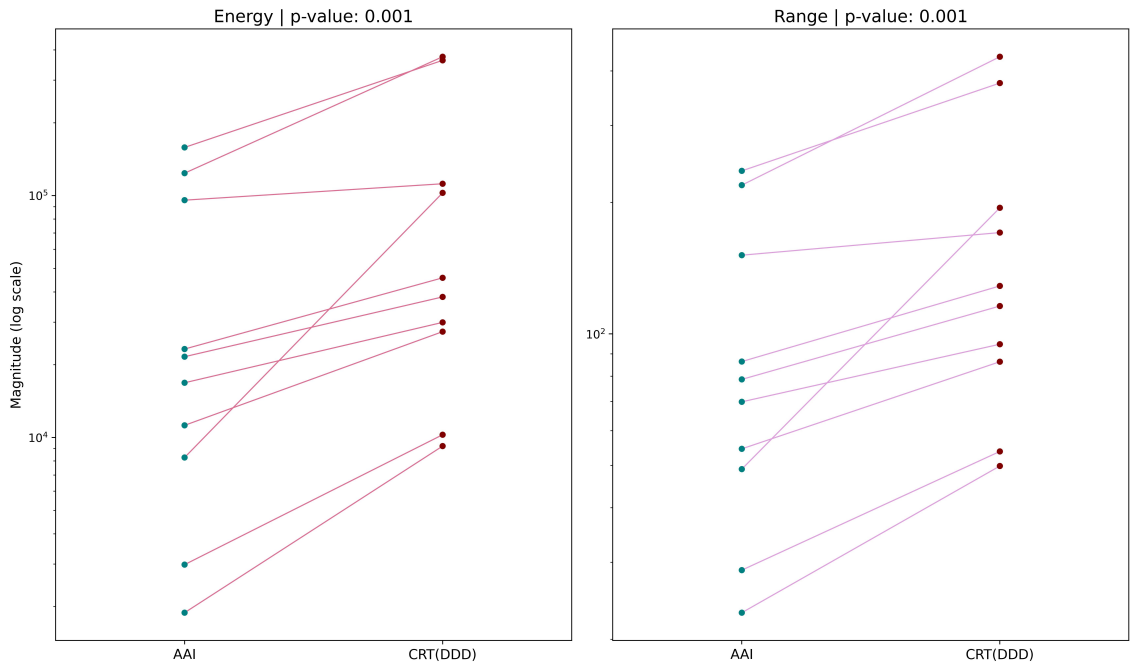

Figure 6.2: Mean systolic energy and range among subject during CRT and AAI mode extracted with AO point synchronization method in the 20-90 Hz range. This illustration originates from the original figure featured in the article [34] and is being used with permission.

7 Discussion

With the introduction of CRT pacing, significant changes around the systolic window were observed in all axes and frequency ranges. During CRT pacing mode, MCG waveforms in the systolic window exhibited higher energy and vertical range. Changes in the waveform were more remarkable in the higher frequency components, with the most concordant differences observed in the 6-90 Hz range. Vertical range variances were clearer than energy differences, specifically; the differences detected in the vertical range were significant in a wider range of frequency ranges and axes. The best axes for observing differences were SCG-Y, GCG-X, and GCG-Y, and the GCG vector outperformed the SCG vector in showing differences. As shown in Fig. 6.2, all heart failure patients showed a consistent increase in vertical range and energy when the pacing mode changed to CRT from AAI. R-peak synchronization and AO point synchronization methods produced similar results while showing differences in a slightly different experiment set. However, no consistent differences were observed in the vertical range and energy around the early diastolic window after the introduction of resynchronization pacing, and there were no significant differences in the LVET and QS2 parameters measured during CRT and AAI mode.

Cardiac resynchronization therapy (CRT) can enhance cardiac function by synchronizing ventricular contraction, resulting in an elevated left ventricular ejection fraction, cardiac index, rapid rate of pressure rise, and decreased left ventricular end-systolic volume index [13], [14], [129]–[132]. Through reverse modeling, CRT

has been shown to reduce the rate of death and hospitalization in selected heart failure with reduced ejection fraction (HFrEF) patients [132]–[134]. Existing literature indicates that CRT pacing mode leads to better cardiac function than AAI pacing mode [135]. Additionally, signals such as seismocardiography (SCG) and gyrocardiography (GCG) have been demonstrated to encompass information regarding cardiac performance. MCG waveforms, specifically, are proposed to reflect left ventricular contractility, left ventricular stroke volume, and improved cardiac performance [26], [29], [65], [116], [136], [137].

Building upon methodologies used to analyze SCG and GCG measurements and the proposed relationships between MCG features and cardiac contractility in the literature, energy (E_x) and vertical range (R_x) features were defined to reflect contraction characteristics in the systolic and early diastolic phases. Consistently, in the three sets of CRT-AAI segments, energy and vertical range around the systolic window showed a statistically significant increase in our patient cohort when the pacemaker mode changed from AAI to CRT. Based on the established relationship between MCG magnitude characteristics and cardiac contractility, as well as the link between CRT pacing and improved cardiac function, it can be proposed that the observed increase in vertical range and energy is related to the improvement of ventricular function resulting from CRT pacing. This suggests a potential application of MCG signals for the assessment and prediction of CRT response in heart failure patients.

Heart sounds offer crucial insights into heart function and contribute to the diagnosis of diverse cardiac conditions [60], [138]–[142]. Specifically, the intensity of the first heart sound (S1) correlates with cardiac contractility and cardiac reserve, and a diminished S1 sound serves as a clinical marker for heart failure [143]–[146]. Acoustic vibrations related to heart sounds emerge in the higher frequency components of MCG signals, and in our study, the most concordant changes were observed

by including higher frequency components.

Observed changes in systolic features when pacemaker mode changed to CRT mode were most prominent in the GCG axes and GCG vector. This is consistent with the previous observations, which proposed that GCG signals exhibit lower sensitivity to both inter-subject and intra-subject variations compared to SCG, particularly in the GCG-X and GCG-Y axes [23], [25], [32], [147], [148]. GCG-Z axis, however, generally has lower signal quality than other GCG axes and showed less salient results in our analysis [23]. Among the SCG axes, the SCG-Y axis showed the most concordant results, including vibrations in the foot-to-head direction of blood movements.

The vertical range feature exhibited statistical differences in a broader range of experiments compared to the energy feature. It is important to note that the vertical range calculation employs only extrema points within the selected window, whereas the energy calculation encompasses every point, as depicted in Figure 5.4. Utilizing every sample in the window may render the energy feature more susceptible to noise and alterations in values. Conversely, the vertical range calculation considers only extrema points that shows distinctive morphologies and potentially offers greater reliability.

Synchronized averaging includes the alignment of all heart beats according to the selected reference and getting the average of the heart beats with respect to this alignment. Different axes of the MCG measurements follow special shapes (peaks and valleys) for various hemodynamic events, and these waveform morphologies are annotated and defined in the literature [23], [55]. It is important to note that the reference point may have an effect on the extracted mean beat and the analysis by enhancing some of these shapes or distorting them. This effect of the reference point on the morphology of the interested fiducial point depends on the variability of the time difference between these points. In Figure 7.1, mean GCG-X beats extracted

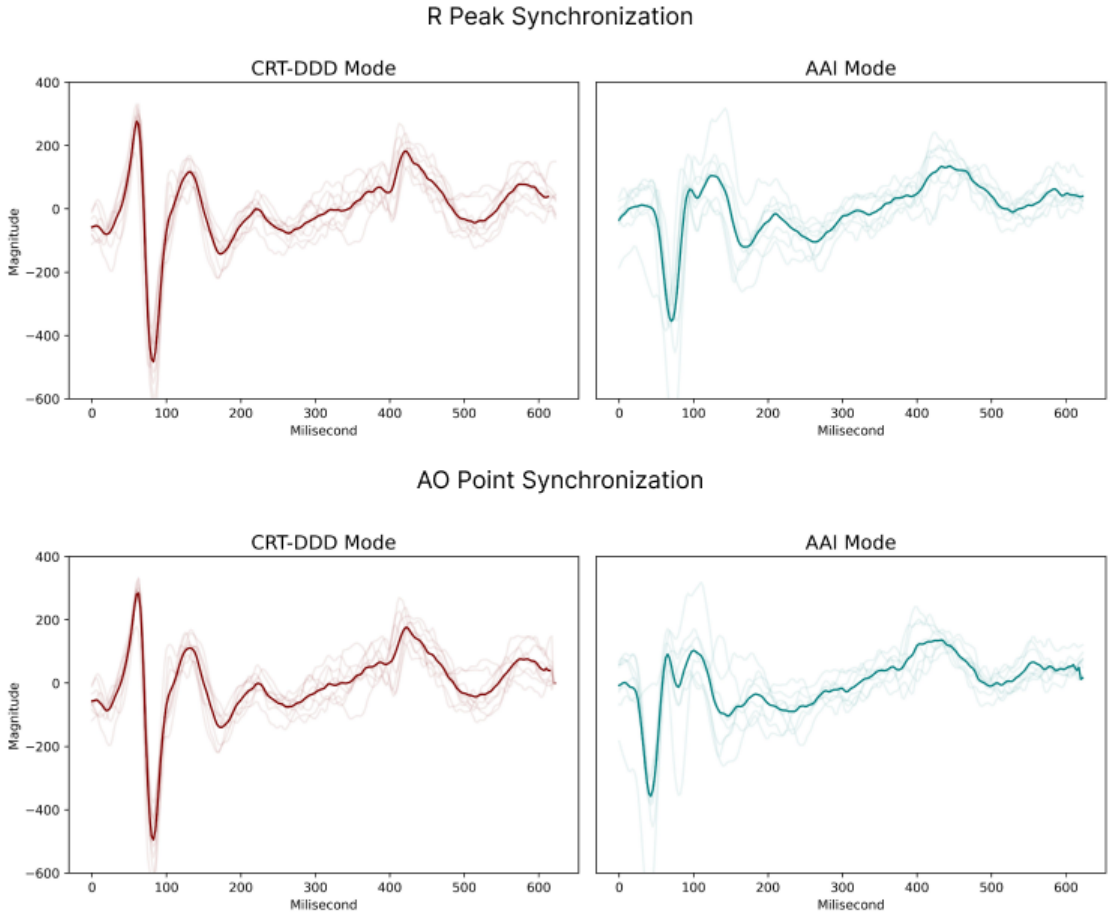

Figure 7.1: Mean GCG-X beats extracted with R peak and AO point synchronization for CRT (left column) and AAI (right column) mode with all individual beats. Individual beats are shown with the lighter colors.

with R peak and AO point synchronization for one subject during CRT and AAI mode are presented with all individual beats, and you can see the differences in the alignment of individual beats and the waveform differences between the resulted mean beats. Also, the effect of the selected reference on SCG waveform analysis is shown in the literature [55]. For this reason, in this study, we employed two different reference points for synchronized averaging and applied the same analysis pipeline using both of them. While their results are generally comparable and consistent, only one of these reference points resulted in significant differences in the SCG-X and GCG-Z axes.

No statistical difference was observed in the early diastolic features when pacing mode was changed from AAI to CRT, in contrast with systolic features. In the literature, it is shown that MCG waveforms can reveal various alterations in cardiac functions and detect abnormalities like heart failure and myocardial infarction [26], [149]–[152]. In addition, it was found that patients with ST elevation myocardial infarction (STEMI) show lower signal strength features in the systolic window than control patients, consistent with our results and machine learning approaches were utilized to detect STEMI [60]. On the other hand, the diagnostic precision of these methodologies is still limited due to inter-subject variability that can be caused by differences in heart orientation and body mass distribution. These variations considerably effect the separability of the healthy controls and patient groups. However, comparing the subject with oneself and detecting the changes with a self-similarity-based approach may be a better approach for detecting abnormalities [24], [26], [153]. Elevated left ventricular filling pressure can be reliably identified with a louder S3 sound [154], and the change in the ventricular filling pressure due to the progression of heart failure is most concordant in the early diastolic waveforms [155]–[158]. In our study, early diastolic features did not change significantly after the resychronization started because more time is needed to see compensatory changes in filling

pressures.

In the literature, it is shown that LVET is shorter in HFrEF patients than in controls, and extended LVET is observed when the pacemaker mode is switched from AAI to CRT [128], [159]. On the other hand, the mean difference between these pacemaker modes was only 6 ms, and this difference was only observable with impedance cardiography but not with echocardiography [128]. In contrast to the reported difference, we could not identify any differences in LVET and QS2 between the two modes. Based on the variations in results acquired through different measurement methods, it is important to analyze our measurement unit. Firstly, the sampling rate of our sensors was 400 Hz, and a limited sampling rate could be a potential obstacle for sensitive measurement of timing parameters and detecting differences in LVET and QS2, considering the low mean difference between the two groups. Furthermore, studies using SCG at 2000 Hz and 5000 Hz reported that there is no significant difference in LVET between the CRT on-off settings and CRT–AAI pacing [29], [160]. Therefore, even though the impact of the CRT mode on systolic performance is evident in MCG, its influence on timing parameters remains unclear and necessitates further examination.

The study faced a significant constraint due to the restricted number of patients. Initially, we had to employ various statistical analyses on the same patient group, a process typically necessitating p-value correction [161]. However, the limitation in the number of subjects also constrains the obtained p-values, potentially leading to a attenuation of the observed differences when applying p-value correction. To address this issue, we developed a data analysis algorithm that iterates the same test on three pairs acquired from different time points. The alternative hypothesis was accepted only if all three pairs exhibited statistically significant results. This method introduced a double-check mechanism to our tests, effectively mitigating time-dependent false-positive results.

Sympathetic activity pertains to the activation of the sympathetic nervous system, leading to heightened physiological responses, including an elevated heart rate, increased blood pressure, enhanced release of adrenaline, and increased alertness. Variations in sympathetic activity within clinical settings may induce changes in the features computed from SCG and GCG, influencing the observed findings [162]. Additionally, these effects might introduce alterations even in healthy subjects, and it is important to distinguish them from the effects of CRT and validate our results. Therefore, future studies should focus on comparing these variations between healthy controls and HFrEF patients.

In our study, 1-channel ECG measurements recorded simultaneously with MCG were utilized to detect individual heartbeats and enhance the accuracy of fiducial point detection. Although the waveform annotations for aortic valve opening and closing on SCG and GCG signals were defined in the literature [23], [55], the morphology of MCG measurements can undergo significant alterations due to interpersonal variabilities, subject motion, or environmental artifacts [55]. These changes can easily impede the accurate detection of these fiducial points. However, the detection of the R-peak was more convenient because of the distinctive morphology of the R-peak, which differentiates itself with a much higher magnitude and steeper slope from other peaks, and the lower possibility of artifacts in our experimental setting. In our study, it was crucial to properly detect fiducial points for an accurate evaluation of the systolic and early diastolic regions, and we utilized ECG measurements for fiducial point detection. On the other hand, for the implementation of wearable systems that only rely on MCG measurements, it is crucial to develop algorithms that perform fiducial point detection without depending on ECG.

One strength of our study was maintaining a consistent heart rate of 80 bpm throughout the MCG recordings. This constancy was important, particularly in the comparison of LVET and QS2, as changes in heart rate could potentially impact

these parameters [99]. Additionally, the experimental design incorporated stable and undisturbed conditions, with quiet breathing, and aimed to minimize signal interference caused by respiratory sounds and other variations that could potentially affect the accuracy of hypothesis testing.

8 Conclusion

In this thesis, we conducted an analysis of MCG waveforms in HFrEF patients undergoing CRT pacing mode and AAI pacing. CRT pacing, involving ventricular synchronization, demonstrated significantly higher energy and vertical range features compared to AAI pacing and indicated improved mechanical cardiac function. No significant differences were found in waveform features around the early diastolic window, LVET, and QS2 between pacing modes.

Our results suggest that mechanical signals measured on the lower chest wall through accelerometers and gyroscopes show substantial changes during CRT pacing and reflects an enhancement in mechanical cardiac function due to resynchronization therapy.

The advancements in Micro Electro Mechanical Systems (MEMS) have led to the development of capable wearable devices, such as MCG, based on MEMS accelerometers and gyroscopes. The widespread availability of smart devices with MEMS units and growing evidence of MCG's potential utilities make it a promising technology for clinical applications.

The thesis demonstrates the capability of MCG waveforms in showing improvements in cardiac function and offers promise for predicting clinical responses to CRT, optimizing CRT procedures, and facilitating post-implementation follow-ups. However, the study's limitation in the number of subjects necessitates larger patient cohorts for validation and a more comprehensive exploration of MCG's utility for

heart failure patients.

Furthermore, future studies can focus on MCG signals collected via smartphones, developing analysis pipelines for these devices to contribute to the advancement of health monitoring applications in home settings.

References

[1] C. W. Tsao, A. W. Aday, Z. I. Almarzooq, *et al.*, "Heart disease and stroke statistics—2023 update: A report from the american heart association", *Circulation*, vol. 147, no. 8, e93–e621, 2023.

[2] *Centers for disease control and prevention and national center for health statistics*, Jan. 2024. [Online]. Available: `https://www.cdc.gov/nchs/nhanes/`.

[3] N. C. for Health Statistics *et al.*, "Selected circulatory diseases among adults aged 18 and over, by selected characteristics: United states, 2018", *vol*, vol. 6, pp. 1–9, 2018.

[4] S. Irawati, R. Wasir, A. Floriaan Schmidt, *et al.*, "Long-term incidence and risk factors of cardiovascular events in asian populations: Systematic review and meta-analysis of population-based cohort studies", *Current Medical Research and Opinion*, vol. 35, no. 2, pp. 291–299, 2019.

[5] P. A. Heidenreich, B. Bozkurt, D. Aguilar, *et al.*, "2022 aha/acc/hfsa guideline for the management of heart failure: A report of the american college of cardiology/american heart association joint committee on clinical practice guidelines", *Journal of the American College of Cardiology*, vol. 79, no. 17, e263–e421, 2022.

[6] P. A. Heidenreich, N. M. Albert, L. A. Allen, *et al.*, "Forecasting the impact of heart failure in the united states: A policy statement from the american heart association", *Circulation: Heart Failure*, vol. 6, no. 3, pp. 606–619, 2013.

[7] S. M. Dunlay, S. A. Weston, S. J. Jacobsen, and V. L. Roger, "Risk factors for heart failure: A population-based case-control study", *The American journal of medicine*, vol. 122, no. 11, pp. 1023–1028, 2009.

[8] J. E. Ho, D. Enserro, F. P. Brouwers, *et al.*, "Predicting heart failure with preserved and reduced ejection fraction: The international collaboration on heart failure subtypes", *Circulation: Heart Failure*, vol. 9, no. 6, e003116, 2016.

[9] M. Merlo, A. Pivetta, B. Pinamonti, *et al.*, "Long-term prognostic impact of therapeutic strategies in patients with idiopathic dilated cardiomyopathy: Changing mortality over the last 30 years", *European journal of heart failure*, vol. 16, no. 3, pp. 317–324, 2014.

[10] C. Balla and R. Cappato, "When to choose cardiac resynchronization therapy in chronic heart failure: Type and duration of the conduction delay", *European Heart Journal Supplements*, vol. 21, no. Supplement_B, B31–B35, 2019.

[11] C. Linde, K. Ellenbogen, and F. A. McAlister, "Cardiac resynchronization therapy (crt): Clinical trials, guidelines, and target populations", *Heart Rhythm*, vol. 9, no. 8, S3–S13, 2012.

[12] May 2023. [Online]. Available: `https://www.heart.org/en/health-topics/heart-attack/diagnosing-a-heart-attack/electrocardiogram-ecg-or-ekg`.

[13] M. R. Bristow, L. A. Saxon, J. Boehmer, *et al.*, "Cardiac-resynchronization therapy with or without an implantable defibrillator in advanced chronic

heart failure", *New England Journal of Medicine*, vol. 350, no. 21, pp. 2140–2150, 2004.

[14] J. G. Cleland, J.-C. Daubert, E. Erdmann, *et al.*, "The effect of cardiac resynchronization on morbidity and mortality in heart failure", *New England Journal of Medicine*, vol. 352, no. 15, pp. 1539–1549, 2005.

[15] A. F. Members, J. J. McMurray, S. Adamopoulos, *et al.*, "Esc guidelines for the diagnosis and treatment of acute and chronic heart failure 2012: The task force for the diagnosis and treatment of acute and chronic heart failure 2012 of the european society of cardiology. developed in collaboration with the heart failure association (hfa) of the esc", *European heart journal*, vol. 33, no. 14, pp. 1787–1847, 2012.

[16] W. Heggermont, A. Auricchio, and M. Vanderheyden, "Biomarkers to predict the response to cardiac resynchronization therapy", *EP Europace*, vol. 21, no. 11, pp. 1609–1620, 2019.

[17] T. F. Chairs, J.-C. Daubert, L. Saxon, *et al.*, "2012 ehra/hrs expert consensus statement on cardiac resynchronization therapy in heart failure: Implant and follow-up recommendations and management: A registered branch of the european society of cardiology (esc), and the heart rhythm society; and in collaboration with the heart failure society of america (hfsa), the american society of echocardiography (ase), the american heart association (aha), the european association of echocardiography (eae) of the esc and the heart failure association of the esc (hfa).", *Europace*, vol. 14, no. 9, pp. 1236–1286, 2012.

[18] J. G. Cleland, N. Freemantle, J.-C. Daubert, W. Toff, F. Leisch, and L. Tavazzi, "Long-term effect of cardiac resynchronisation in patients reporting mild symptoms of heart failure: A report from the care-hf study", *Heart*, 2007.

[19] A. Auricchio and F. W. Prinzen, "Non-responders to cardiac resynchronization therapy", *Circulation Journal*, vol. 75, 2011.

[20] D. M. Salerno, "Seismocardiography: A new technique for recording cardiac vibrations. concept, method, and initial observations", *Journal of cardiovascular technology*, vol. 9, no. 2, pp. 111–118, 1990.

[21] B. S. Bozhenko, "Seismocardiography–a new method in the study of functional conditions of the heart", *Terapevticheskii arkhiv*, vol. 33, pp. 55–64, 1961.

[22] U. Meriheinä, M. Juppo, T. Koivisto, M. Pänäälä, K. Sairanen, and M. Grönholm, *Heart monitoring system*, US Patent 10,178,964, Jan. 2019.

[23] M. Jafari Tadi, E. Lehtonen, A. Saraste, *et al.*, "Gyrocardiography: A new non-invasive monitoring method for the assessment of cardiac mechanics and the estimation of hemodynamic variables", *Scientific reports*, vol. 7, no. 1, p. 6823, 2017.

[24] T. Koivisto, O. Lahdenoja, T. Hurnanen, *et al.*, "Mechanocardiography-based measurement system indicating changes in heart failure patients during hospital admission and discharge", *Sensors*, vol. 22, no. 24, p. 9781, 2022.

[25] M. J. Tadi, E. Lehtonen, M. Pankäälä, *et al.*, "Gyrocardiography: A new non-invasive approach in the study of mechanical motions of the heart. concept, method and initial observations", in *2016 38th Annual International Conference of the IEEE engineering in medicine and biology society (EMBC)*, IEEE, 2016, pp. 2034–2037.

[26] S. Morra, L. Pitisci, F. Su, *et al.*, "Quantification of cardiac kinetic energy and its changes during transmural myocardial infarction assessed by multidimensional seismocardiography", *Frontiers in Cardiovascular Medicine*, vol. 8, p. 603 319, 2021.

[27] A. Taebi, B. E. Solar, A. J. Bomar, R. H. Sandler, and H. A. Mansy, "Recent advances in seismocardiography", *Vibration*, vol. 2, no. 1, pp. 64–86, 2019.

[28] P. Dehkordi, F. Khosrow-Khavar, M. Di Rienzo, *et al.*, "Comparison of different methods for estimating cardiac timings: A comprehensive multimodal echocardiography investigation", *Frontiers in physiology*, vol. 10, p. 1057, 2019.

[29] K. Sørensen, P. Søgaard, K. Emerek, A. S. Jensen, J. J. Struijk, and S. E. Schmidt, "Seismocardiography as a tool for assessment of bi-ventricular pacing", *Physiological Measurement*, vol. 43, no. 10, p. 105 007, 2022.

[30] A. Agam, P. Søgaard, K. Kragholm, *et al.*, "Correlation between diastolic seismocardiography variables and echocardiography variables", *European Heart Journal-Digital Health*, vol. 3, no. 3, pp. 465–472, 2022.

[31] T. Hurnanen, E. Lehtonen, M. J. Tadi, *et al.*, "Automated detection of atrial fibrillation based on time–frequency analysis of seismocardiograms", *IEEE Journal of Biomedical and Health Informatics*, vol. 21, no. 5, pp. 1233–1241, 2016.

[32] O. Lahdenoja, T. Hurnanen, Z. Iftikhar, *et al.*, "Atrial fibrillation detection via accelerometer and gyroscope of a smartphone", *IEEE Journal of Biomedical and Health Informatics*, vol. 22, no. 1, pp. 108–118, 2017.

[33] M. Becker, A. Roehl, U. Siekmann, *et al.*, "Simplified detection of myocardial ischemia by seismocardiography", *Herz*, vol. 39, no. 5, p. 586, 2014.

[34] F. Tokmak, T. Koivisto, O. Lahdenoja, T. Vasankari, S. Jaakkola, and K. J. Airaksinen, "Mechanocardiography detects improvement of systolic function caused by resynchronization pacing", *Physiological Measurement*, vol. 44, no. 12, p. 125 009, 2023.

[35] S. Doris, D. T. Lee, J. Woo, and D. R. Thompson, "Correlates of psychological distress in elderly patients with congestive heart failure", *Journal of psychosomatic research*, vol. 57, no. 6, pp. 573–581, 2004.

[36] I. Ekman, J. G. Cleland, K. Swedberg, A. Charlesworth, M. Metra, and P. A. Poole-Wilson, "Symptoms in patients with heart failure are prognostic predictors: Insights from comet", *Journal of cardiac failure*, vol. 11, no. 4, pp. 288–292, 2005.

[37] C. D. Kemp and J. V. Conte, "The pathophysiology of heart failure", *Cardiovascular Pathology*, vol. 21, no. 5, pp. 365–371, 2012.

[38] T. A. Foley, S. V. Mankad, N. S. Anavekar, *et al.*, "Measuring left ventricular ejection fraction-techniques and potential pitfalls", *Eur Cardiol*, vol. 8, no. 2, pp. 108–114, 2012.

[39] S. Iuliano, S. G. Fisher, P. E. Karasik, R. D. Fletcher, S. N. Singh, D. of Veterans Affairs Survival Trial of Antiarrhythmic Therapy in Congestive Heart Failure, *et al.*, "Qrs duration and mortality in patients with congestive heart failure", *American heart journal*, vol. 143, no. 6, pp. 1085–1091, 2002.

[40] S. Baldasseroni, C. Opasich, M. Gorini, *et al.*, "Left bundle-branch block is associated with increased 1-year sudden and total mortality rate in 5517 outpatients with congestive heart failure: A report from the italian network on congestive heart failure", *American heart journal*, vol. 143, no. 3, pp. 398–405, 2002.

[41] H. J. Shenkman, V. Pampati, A. K. Khandelwal, *et al.*, "Congestive heart failure and qrs duration: Establishing prognosis study", *Chest*, vol. 122, no. 2, pp. 528–534, 2002.

[42] M. Glikson, J. C. Nielsen, M. B. Kronborg, *et al.*, "2021 esc guidelines on cardiac pacing and cardiac resynchronization therapy: Developed by the task

force on cardiac pacing and cardiac resynchronization therapy of the european society of cardiology (esc) with the special contribution of the european heart rhythm association (ehra)", *EP Europace*, vol. 24, no. 1, pp. 71–164, 2022.

[43] W. T. Abraham, J. B. Young, A. R. León, *et al.*, "Effects of cardiac resynchronization on disease progression in patients with left ventricular systolic dysfunction, an indication for an implantable cardioverter-defibrillator, and mildly symptomatic chronic heart failure", *Circulation*, vol. 110, no. 18, pp. 2864–2868, 2004.

[44] A. Auricchio, C. Stellbrink, S. Sack, *et al.*, "Long-term clinical effect of hemodynamically optimized cardiac resynchronization therapy in patients with heart failure and ventricular conduction delay", *Journal of the American College of Cardiology*, vol. 39, no. 12, pp. 2026–2033, 2002.

[45] J. G. Cleland, J.-C. Daubert, E. Erdmann, *et al.*, "Longer-term effects of cardiac resynchronization therapy on mortality in heart failure [the cardiac resynchronization-heart failure (care-hf) trial extension phase]", *European heart journal*, vol. 27, no. 16, pp. 1928–1932, 2006.

[46] C. Linde, W. T. Abraham, M. R. Gold, *et al.*, "Randomized trial of cardiac resynchronization in mildly symptomatic heart failure patients and in asymptomatic patients with left ventricular dysfunction and previous heart failure symptoms", *Journal of the American College of Cardiology*, vol. 52, no. 23, pp. 1834–1843, 2008.

[47] E. S. Chung, A. R. Leon, L. Tavazzi, *et al.*, "Results of the predictors of response to crt (prospect) trial", *Circulation*, vol. 117, no. 20, pp. 2608–2616, 2008.

[48] J. Cleland, N. Freemantle, S. Ghio, *et al.*, "Predicting the long-term effects of cardiac resynchronization therapy on mortality from baseline variables and

the early response: A report from the care-hf (cardiac resynchronization in heart failure) trial", *Journal of the American College of Cardiology*, vol. 52, no. 6, pp. 438–445, 2008.

[49] Y. D'Mello, J. Skoric, S. Xu, *et al.*, "Real-time cardiac beat detection and heart rate monitoring from combined seismocardiography and gyrocardiography", *Sensors*, vol. 19, no. 16, p. 3472, 2019.

[50] A. Taebi, B. E. Solar, A. J. Bomar, R. H. Sandler, and H. A. Mansy, "Recent advances in seismocardiography", *Vibration*, vol. 2, no. 1, pp. 64–86, 2019, ISSN: 2571-631X. DOI: 10.3390/vibration2010005. [Online]. Available: https://www.mdpi.com/2571-631X/2/1/5.

[51] A. Taebi and H. Mansy, "Effect of noise on time-frequency analysis of vibrocardiographic signals", *Journal of bioengineering & biomedical science*, vol. 6, no. 4, 2016.

[52] O. T. Inan, P.-F. Migeotte, K.-S. Park, *et al.*, "Ballistocardiography and seismocardiography: A review of recent advances", *IEEE journal of biomedical and health informatics*, vol. 19, no. 4, pp. 1414–1427, 2014.

[53] V. Gurev, K. Tavakolian, J. Constantino, B. Kaminska, A. P. Blaber, and N. A. Trayanova, "Mechanisms underlying isovolumic contraction and ejection peaks in seismocardiogram morphology", *Journal of medical and biological engineering*, vol. 32, no. 2, p. 103, 2012.

[54] R. S. Crow, P. Hannan, D. Jacobs, L. Hedquist, and D. M. Salerno, "Relationship between seismocardiogram and echocardiogram for events in the cardiac cycle", *American journal of noninvasive cardiology*, vol. 8, no. 1, pp. 39–46, 1994.

[55] K. Sørensen, S. E. Schmidt, A. S. Jensen, P. Søgaard, and J. J. Struijk, "Definition of fiducial points in the normal seismocardiogram", *Scientific reports*, vol. 8, no. 1, p. 15 455, 2018.

[56] M. J. Tadi, T. Koivisto, M. Pänkäälä, *et al.*, "A new algorithm for segmentation of cardiac quiescent phases and cardiac time intervals using seismocardiography", in *Sixth International Conference on Graphic and Image Processing (ICGIP 2014)*, SPIE, vol. 9443, 2015, pp. 571–577.

[57] K. Tavakolian, "Characterization and analysis of seismocardiogram for estimation of hemodynamic parameters", 2010.

[58] P. Reant, M. Dijos, E. Donal, *et al.*, "Systolic time intervals as simple echocardiographic parameters of left ventricular systolic performance: Correlation with ejection fraction and longitudinal two-dimensional strain", *European Journal of Echocardiography*, vol. 11, no. 10, pp. 834–844, 2010.

[59] H. Boudoulas, "Systolic time intervals", *European heart journal*, vol. 11, no. suppl_I, pp. 93–104, 1990.

[60] T. Koivisto, O. Lahdenoja, T. Hurnanen, *et al.*, "Mechanocardiography in the detection of acute st elevation myocardial infarction: The mechano-stemi study", *Sensors*, vol. 22, no. 12, p. 4384, 2022.

[61] D. Rai, H. K. Thakkar, S. S. Rajput, J. Santamaria, C. Bhatt, and F. Roca, "A comprehensive review on seismocardiogram: Current advancements on acquisition, annotation, and applications", *Mathematics*, vol. 9, no. 18, p. 2243, 2021.

[62] F. Tokmak and B. Semiz, "Unveiling the relationships between seismocardiogram signals, physical activity types and metabolic equivalent of task scores", *IEEE Transactions on Biomedical Engineering*, vol. 70, no. 2, pp. 479–487, 2022.

[63] D. S. Morillo, J. L. R. Ojeda, L. F. C. Foix, and A. L. Jiménez, "An accelerometer-based device for sleep apnea screening", *IEEE transactions on information technology in biomedicine*, vol. 14, no. 2, pp. 491–499, 2009.

[64] B. Semiz, A. M. Carek, J. C. Johnson, *et al.*, "Non-invasive wearable patch utilizing seismocardiography for peri-operative use in surgical patients", *IEEE journal of biomedical and health informatics*, vol. 25, no. 5, pp. 1572–1582, 2020.

[65] P. Castiglioni, A. Faini, G. Parati, and M. Di Rienzo, "Wearable seismocardiography", in *2007 29th annual international conference of the IEEE engineering in medicine and biology society*, IEEE, 2007, pp. 3954–3957.

[66] C. S. Spencer *et al.*, "Nurses with undiagnosed hearing loss: Implications for practice", *Online Journal of Issues in Nursing*, vol. 20, no. 1, p. 56, 2015.

[67] A. L. Goldberger, Z. D. Goldberger, and A. Shvilkin, "Chapter 4 - ecg leads", in *Goldberger's Clinical Electrocardiography (Ninth Edition)*, A. L. Goldberger, Z. D. Goldberger, and A. Shvilkin, Eds., Ninth Edition, Elsevier, 2018, pp. 21–31, ISBN: 978-0-323-40169-2. DOI: https://doi.org/10.1016/B978-0-323-40169-2.00004-4. [Online]. Available: https://www.sciencedirect.com/science/article/pii/B9780323401692000044.

[68] A. L. Goldberger, Z. D. Goldberger, and A. Shvilkin, "Chapter 2 - ecg basics: Waves, intervals, and segments", in *Goldberger's Clinical Electrocardiography (Ninth Edition)*, A. L. Goldberger, Z. D. Goldberger, and A. Shvilkin, Eds., Ninth Edition, Elsevier, 2018, pp. 6–10, ISBN: 978-0-323-40169-2. DOI: https://doi.org/10.1016/B978-0-323-40169-2.00002-0. [Online]. Available: https://www.sciencedirect.com/science/article/pii/B9780323401692000020.

[69] T. Reichlin, R. Abächerli, R. Twerenbold, *et al.*, "Advanced ecg in 2016: Is there more than just a tracing?", *Swiss medical weekly*, vol. 146, no. 1718, w14303–w14303, 2016.

[70] N. Rafie, A. H. Kashou, and P. A. Noseworthy, "Ecg interpretation: Clinical relevance, challenges, and advances", *Hearts*, vol. 2, no. 4, pp. 505–513, 2021.

[71] Y. Yoon, J. H. Cho, and G. Yoon, "Non-constrained blood pressure monitoring using ecg and ppg for personal healthcare", *Journal of medical systems*, vol. 33, pp. 261–266, 2009.

[72] P. Hamilton, "Open source ecg analysis", in *Computers in cardiology*, IEEE, 2002, pp. 101–104.

[73] J. Pan and W. J. Tompkins, "A real-time qrs detection algorithm", *IEEE transactions on biomedical engineering*, no. 3, pp. 230–236, 1985.

[74] J. P. Martínez, R. Almeida, S. Olmos, A. P. Rocha, and P. Laguna, "A wavelet-based ecg delineator: Evaluation on standard databases", *IEEE Transactions on biomedical engineering*, vol. 51, no. 4, pp. 570–581, 2004.

[75] F. Emmert-Streib and M. Dehmer, "Understanding statistical hypothesis testing: The logic of statistical inference", *Machine Learning and Knowledge Extraction*, vol. 1, no. 3, pp. 945–962, 2019.

[76] J. Neyman and E. S. Pearson, "Ix. on the problem of the most efficient tests of statistical hypotheses", *Philosophical Transactions of the Royal Society of London. Series A, Containing Papers of a Mathematical or Physical Character*, vol. 231, no. 694-706, pp. 289–337, 1933.

[77] Student, "The probable error of a mean", *Biometrika*, vol. 6, no. 1, pp. 1–25, 1908, ISSN: 00063444. [Online]. Available: `http://www.jstor.org/stable/2331554` (visited on 03/17/2024).

[78] F. Galton, *Natural inheritance*. Macmillan, 1889, vol. 42.

[79] H. B. Mann and D. R. Whitney, "On a Test of Whether one of Two Random Variables is Stochastically Larger than the Other", *The Annals of Mathematical Statistics*, vol. 18, no. 1, pp. 50–60, 1947. DOI: 10.1214/aoms/1177730491. [Online]. Available: https://doi.org/10.1214/aoms/1177730491.

[80] F. Wilcoxon, "Individual comparisons by ranking methods", in *Breakthroughs in Statistics: Methodology and Distribution*, Springer, 1992, pp. 196–202.

[81] W. H. Kruskal and W. A. Wallis, "Use of ranks in one-criterion variance analysis", *Journal of the American Statistical Association*, vol. 47, no. 260, pp. 583–621, 1952. DOI: 10.1080/01621459.1952.10483441. eprint: https://www.tandfonline.com/doi/pdf/10.1080/01621459.1952.10483441. [Online]. Available: https://www.tandfonline.com/doi/abs/10.1080/01621459.1952.10483441.

[82] D. Sundararajan, *Digital signal processing: theory and practice*. World Scientific, 2003.

[83] A. Averbuch, D. Lazar, and M. Israeli, "Image compression using wavelet transform and multiresolution decomposition", *IEEE Transactions on Image Processing*, vol. 5, no. 1, pp. 4–15, 1996.

[84] Q. Pan, L. Zhang, G. Dai, and H. Zhang, "Two denoising methods by wavelet transform", *IEEE transactions on signal processing*, vol. 47, no. 12, pp. 3401–3406, 1999.

[85] Q. Zhao and L. Zhang, "Ecg feature extraction and classification using wavelet transform and support vector machines", in *2005 International Conference on Neural Networks and Brain*, IEEE, vol. 2, 2005, pp. 1089–1092.

[86] A. N. Akansu, W. A. Serdijn, and I. W. Selesnick, "Emerging applications of wavelets: A review", *Physical communication*, vol. 3, no. 1, pp. 1–18, 2010.

[87] V. N. Varghees and K. Ramachandran, "Effective heart sound segmentation and murmur classification using empirical wavelet transform and instantaneous phase for electronic stethoscope", *IEEE Sensors Journal*, vol. 17, no. 12, pp. 3861–3872, 2017.

[88] L. Huiying, L. Sakari, and H. Iiro, "A heart sound segmentation algorithm using wavelet decomposition and reconstruction", in *Proceedings of the 19th Annual International Conference of the IEEE Engineering in Medicine and Biology Society. 'Magnificent Milestones and Emerging Opportunities in Medical Engineering' (Cat. No.97CH36136)*, vol. 4, 1997, 1630–1633 vol.4. DOI: 10.1109/IEMBS.1997.757028.

[89] T. Choudhary, L. Sharma, and M. K. Bhuyan, "Automatic detection of aortic valve opening using seismocardiography in healthy individuals", *IEEE journal of biomedical and health informatics*, vol. 23, no. 3, pp. 1032–1040, 2018.

[90] T. Choudhary, L. Sharma, and M. K. Bhuyan, "Heart sound extraction from sternal seismocardiographic signal", *IEEE Signal Processing Letters*, vol. 25, no. 4, pp. 482–486, 2018.

[91] M. A. García-González, A. Argelagós-Palau, M. Fernández-Chimeno, and J. Ramos-Castro, "A comparison of heartbeat detectors for the seismocardiogram", in *Computing in Cardiology 2013*, 2013, pp. 461–464.

[92] B. Ergen, Y. Tatar, and H. O. Gulcur, "Time–frequency analysis of phonocardiogram signals using wavelet transform: A comparative study", *Computer methods in biomechanics and biomedical engineering*, vol. 15, no. 4, pp. 371–381, 2012.

[93] T. Oskiper and R. Watrous, "Detection of the first heart sound using a time-delay neural network", in *Computers in Cardiology*, IEEE, 2002, pp. 537–540.

[94] L. Huiying, L. Sakari, and H. Iiro, "A heart sound segmentation algorithm using wavelet decomposition and reconstruction", in *Proceedings of the 19th Annual International Conference of the IEEE Engineering in Medicine and Biology Society.'Magnificent Milestones and Emerging Opportunities in Medical Engineering'(Cat. No. 97CH36136)*, IEEE, vol. 4, 1997, pp. 1630–1633.

[95] C. N. Gupta, R. Palaniappan, S. Swaminathan, and S. M. Krishnan, "Neural network classification of homomorphic segmented heart sounds", *Applied soft computing*, vol. 7, no. 1, pp. 286–297, 2007.

[96] K. Pandia, O. T. Inan, G. T. Kovacs, and L. Giovangrandi, "Extracting respiratory information from seismocardiogram signals acquired on the chest using a miniature accelerometer", *Physiological measurement*, vol. 33, no. 10, p. 1643, 2012.

[97] I. Elnaggar, J. Pykäri, T. Hurnanen, *et al.*, "Cardiac time intervals derived from electrocardiography and seismocardiography in different patient groups", in *2022 Computing in Cardiology (CinC)*, vol. 498, 2022, pp. 1–4. DOI: 10.22489/CinC.2022.370.

[98] J. L. Willems, J. Roelandt, H. DE GEEST, H. Kesteloot, and J. V. JOOSSENS, "The left ventricular ejection time in elderly subjects", *Circulation*, vol. 42, no. 1, pp. 37–42, 1970.

[99] A. M. Weissler, L. C. Harris, and G. D. White, "Left ventricular ejection time index in man", *Journal of Applied Physiology*, vol. 18, no. 5, pp. 919–923, 1963.

[100] G. Andelfinger, J.-C. Fouron, S.-E. Sonesson, and F. Proulx, "Reference values for time intervals between atrial and ventricular contractions of the fetal heart measured by two doppler techniques", *American Journal of Cardiology*, vol. 88, no. 12, pp. 1433–1436, 2001.

[101] A. S. Alhakak, F. J. Olsen, K. G. Skaarup, *et al.*, "Age-and sex-based normal reference ranges of the cardiac time intervals: The copenhagen city heart study", *Clinical Research in Cardiology*, pp. 1–13, 2023.

[102] S. Siecinski, E. J. Tkacz, and P. S. Kostka, "Comparison of hrv indices obtained from ecg and scg signals from cebs database", *Biomedical engineering online*, vol. 18, pp. 1–15, 2019.

[103] G. Shafiq, S. Tatinati, and K. C. Veluvolu, "Automatic annotation of peaks in seismocardiogram for systolic time intervals", in *2016 38th Annual International Conference of the IEEE Engineering in Medicine and Biology Society (EMBC)*, IEEE, 2016, pp. 2672–2675.

[104] M. J. Tadi, E. Lehtonen, T. Hurnanen, *et al.*, "A real-time approach for heart rate monitoring using a hilbert transform in seismocardiograms", *Physiological measurement*, vol. 37, no. 11, p. 1885, 2016.

[105] H. Sakoe and S. Chiba, "Dynamic programming algorithm optimization for spoken word recognition", *IEEE transactions on acoustics, speech, and signal processing*, vol. 26, no. 1, pp. 43–49, 1978.

[106] D. J. Berndt and J. Clifford, "Using dynamic time warping to find patterns in time series", in *Proceedings of the 3rd international conference on knowledge discovery and data mining*, 1994, pp. 359–370.

[107] K. Wang and T. Gasser, "Alignment of curves by dynamic time warping", *The annals of Statistics*, vol. 25, no. 3, pp. 1251–1276, 1997.

[108] E. J. Keogh and M. J. Pazzani, "Scaling up dynamic time warping to massive datasets", in *Principles of Data Mining and Knowledge Discovery: Third European Conference, PKDD'99, Prague, Czech Republic, September 15-18, 1999. Proceedings 3*, Springer, 1999, pp. 1–11.

[109] Y.-S. Jeong, M. K. Jeong, and O. A. Omitaomu, "Weighted dynamic time warping for time series classification", *Pattern recognition*, vol. 44, no. 9, pp. 2231–2240, 2011.

[110] M. Yadav and M. A. Alam, "Dynamic time warping (dtw) algorithm in speech: A review", *International Journal of Research in Electronics and Computer Engineering*, vol. 6, no. 1, pp. 524–528, 2018.

[111] C.-H. Chen, W.-Y. Lin, and M.-Y. Lee, "Computer-aided detection of fiducial points in seismocardiography through dynamic time warping", *Biosensors*, vol. 12, no. 6, p. 374, 2022.

[112] B.-J. Yoon, "Hidden markov models and their applications in biological sequence analysis", *Current genomics*, vol. 10, no. 6, pp. 402–415, 2009.

[113] J. Wahlström, I. Skog, P. Händel, *et al.*, "A hidden markov model for seismocardiography", *IEEE Transactions on Biomedical Engineering*, vol. 64, no. 10, pp. 2361–2372, 2017.

[114] B. Semiz, A. M. Carek, J. C. Johnson, *et al.*, "Non-invasive wearable patch utilizing seismocardiography for peri-operative use in surgical patients", *IEEE Journal of Biomedical and Health Informatics*, vol. 25, no. 5, pp. 1572–1582, 2021. DOI: 10.1109/JBHI.2020.3032938.

[115] F. Tokmak and B. Semiz, "Unveiling the relationships between seismocardiogram signals, physical activity types and metabolic equivalent of task scores", *IEEE Transactions on Biomedical Engineering*, vol. 70, no. 2, pp. 479–487, 2023. DOI: 10.1109/TBME.2022.3194594.

[116] V. Gemignani, E. Bianchini, F. Faita, *et al.*, "Transthoracic sensor for non-invasive assessment of left ventricular contractility: Validation in a minipig model of chronic heart failure", *Pacing and clinical electrophysiology*, vol. 33, no. 7, pp. 795–803, 2010.

[117] Z. M. Işilay Zeybek, V. Racca, A. Pezzano, M. Tavanelli, and M. Di Rienzo, "Can seismocardiogram fiducial points be used for the routine estimation of cardiac time intervals in cardiac patients?", *Frontiers in Physiology*, vol. 13, p. 372, 2022.

[118] M. Di Rienzo, E. Vaini, P. Castiglioni, P. Meriggi, and F. Rizzo, "Beat-to-beat estimation of lvet and qs2 indices of cardiac mechanics from wearable seismocardiography in ambulant subjects", in *2013 35th Annual International Conference of the IEEE Engineering in Medicine and Biology Society (EMBC)*, IEEE, 2013, pp. 7017–7020.

[119] A. S. Alhakak, J. R. Teerlink, J. Lindenfeld, M. Böhm, G. M. Rosano, and T. Biering-Sørensen, "The significance of left ventricular ejection time in heart failure with reduced ejection fraction", *European journal of heart failure*, vol. 23, no. 4, pp. 541–551, 2021.

[120] T. Biering-Sørensen, G. Querejeta Roca, S. M. Hegde, *et al.*, "Left ventricular ejection time is an independent predictor of incident heart failure in a community-based cohort", *European journal of heart failure*, vol. 20, no. 7, pp. 1106–1114, 2018.

[121] A. Dodek, J. R. Burg, and F. E. Kloster, "Systolic time intervals in chronic hypertension: Alterations and response to treatment", *Chest*, vol. 68, no. 1, pp. 51–55, 1975.

[122] R. P. Lewis, H. Boudoulas, T. G. Welch, and W. F. Forester, "Usefulness of systolic time intervals in coronary artery disease", *The American journal of cardiology*, vol. 37, no. 5, pp. 787–796, 1976.

[123] W. Chen and D. Gibson, "Mechanisms of prolongation of pre-ejection period in patients with left ventricular disease.", *Heart*, vol. 42, no. 3, pp. 304–310, 1979.

[124] H. Schächinger, M. Weinbacher, A. Kiss, R. Ritz, and W. Langewitz, "Cardiovascular indices of peripheral and central sympathetic activation", *Psychosomatic medicine*, vol. 63, no. 5, pp. 788–796, 2001.

[125] H. Boudoulas, Y. H. Sohn, W. O'neill, R. Brown, and A. M. Weissler, "The qt> qs2 syndrome: A new mortality risk indicator in coronary artery disease", *The American Journal of Cardiology*, vol. 50, no. 6, pp. 1229–1235, 1982.

[126] P. Bifulco, G. Gargiulo, G. d'Angelo, *et al.*, "Monitoring of respiration, seismocardiogram and heart sounds by a pvdf piezo film sensor", *Measurement*, vol. 11, pp. 786–789, 2014.

[127] D. Makowski, T. Pham, Z. J. Lau, *et al.*, "NeuroKit2: A python toolbox for neurophysiological signal processing", *Behavior Research Methods*, vol. 53, no. 4, pp. 1689–1696, Feb. 2021. DOI: 10.3758/s13428-020-01516-y. [Online]. Available: https://doi.org/10.3758%2Fs13428-020-01516-y.

[128] K. Noda, H. Endo, T. Kadosaka, *et al.*, "Comparison of the measured pre-ejection periods and left ventricular ejection times between echocardiography and impedance cardiography for optimizing cardiac resynchronization therapy", *Journal of arrhythmia*, vol. 33, no. 2, pp. 130–133, 2017.

[129] D. J. Friedman, S. M. Al-Khatib, F. Dalgaard, *et al.*, "Cardiac resynchronization therapy improves outcomes in patients with intraventricular conduction delay but not right bundle branch block: A patient-level meta-analysis of randomized controlled trials", *Circulation*, vol. 147, no. 10, pp. 812–823, 2023.

[130] A. S. Tang, G. A. Wells, M. Talajic, *et al.*, "Cardiac-resynchronization therapy for mild-to-moderate heart failure", *New England Journal of Medicine*, vol. 363, no. 25, pp. 2385–2395, 2010.

[131] A. J. Moss, W. J. Hall, D. S. Cannom, *et al.*, "Cardiac-resynchronization therapy for the prevention of heart-failure events", *New England Journal of Medicine*, vol. 361, no. 14, pp. 1329–1338, 2009.

[132] C. Linde, M. R. Gold, W. T. Abraham, *et al.*, "Long-term impact of cardiac resynchronization therapy in mild heart failure: 5-year results from the resynchronization reverses remodeling in systolic left ventricular dysfunction (reverse) study", *European heart journal*, vol. 34, no. 33, pp. 2592–2599, 2013.

[133] P. Steendijk, S. A. Tulner, J. J. Bax, *et al.*, "Hemodynamic effects of long-term cardiac resynchronization therapy: Analysis by pressure-volume loops", *Circulation*, vol. 113, no. 10, pp. 1295–1304, 2006.

[134] C.-M. Yu, E. Chau, J. E. Sanderson, *et al.*, "Tissue doppler echocardiographic evidence of reverse remodeling and improved synchronicity by simultaneously delaying regional contraction after biventricular pacing therapy in heart failure", *Circulation*, vol. 105, no. 4, pp. 438–445, 2002.

[135] C. Leclercq, S. Cazeau, H. Le Breton, *et al.*, "Acute hemodynamic effects of biventricular ddd pacing in patients with end-stage heart failure", *Journal of the American College of Cardiology*, vol. 32, no. 7, pp. 1825–1831, 1998.

[136] P. Bordachar, L. Labrousse, S. Ploux, *et al.*, "Validation of a new noninvasive device for the monitoring of peak endocardial acceleration in pigs: Implications for optimization of pacing site and configuration", *Journal of cardiovascular electrophysiology*, vol. 19, no. 7, pp. 725–729, 2008.

[137] K. Tavakolian, A. P. Blaber, B. Ngai, and B. Kaminska, "Estimation of hemodynamic parameters from seismocardiogram", in *2010 Computing in Cardiology*, IEEE, 2010, pp. 1055–1058.

[138] S. Dornbush and A. E. Turnquest, "Physiology, heart sounds", 2019.

[139] W. P. Harvey, "Heart sounds and murmurs", *Circulation*, vol. 30, no. 2, pp. 262–271, 1964.

[140] S. Schmidt, C. Holst-Hansen, C. Graff, E. Toft, and J. Struijk, "Detection of coronary artery disease with an electronic stethoscope", in *2007 Computers in Cardiology*, IEEE, 2007, pp. 757–760.

[141] E. D. Folland, B. J. Kriegel, W. G. Henderson, K. E. Hammermeister, G. K. Sethi, and P. in the Veterans Affairs Cooperative Study on Valvular Heart Disease*, "Implications of third heart sounds in patients with valvular heart disease", *New England Journal of Medicine*, vol. 327, no. 7, pp. 458–462, 1992.

[142] M. Akay, J. Semmlow, W. Welkowitz, M. Bauer, and J. Kostis, "Detection of coronary occlusions using autoregressive modeling of diastolic heart sounds", *IEEE Transactions on Biomedical Engineering*, vol. 37, no. 4, pp. 366–373, 1990.

[143] P. H. Thakur, Q. An, L. Swanson, Y. Zhang, and R. S. Gardner, "Haemodynamic monitoring of cardiac status using heart sounds from an implanted cardiac device", *ESC Heart Failure*, vol. 4, no. 4, pp. 605–613, 2017.

[144] P. B. Hansen, A. A. Luisada, D. J. Miletich, and R. F. Albrecht, "Phonocardiography as a monitor of cardiac performance during anesthesia", *Anesthesia & Analgesia*, vol. 68, no. 3, pp. 385–387, 1989.

[145] S. Xiao, X. Guo, X. Sun, and Z. Xiao, "A relative value method for measuring and evaluating cardiac reserve", *Biomedical engineering online*, vol. 1, no. 1, pp. 1–5, 2002.

[146] Y. Zheng, X. Guo, J. Qin, and S. Xiao, "Computer-assisted diagnosis for chronic heart failure by the analysis of their cardiac reserve and heart sound characteristics", *Computer methods and programs in biomedicine*, vol. 122, no. 3, pp. 372–383, 2015.

[147] M. J. Tadi, E. Lehtonen, J. Teuho, *et al.*, "A miniaturized mems motion processing system for nuclear medicine imaging applications", in *2016 Computing in Cardiology Conference (CinC)*, IEEE, 2016, pp. 133–136.

[148] O. Lahdenoja, T. Humanen, M. J. Tadi, M. Pänkäälä, and T. Koivisto, "Heart rate variability estimation with joint accelerometer and gyroscope sensing", in *2016 Computing in Cardiology Conference (CinC)*, IEEE, 2016, pp. 717–720.

[149] O. T. Inan, M. Baran Pouyan, A. Q. Javaid, *et al.*, "Novel wearable seismocardiography and machine learning algorithms can assess clinical status of heart failure patients", *Circulation: Heart Failure*, vol. 11, no. 1, e004313, 2018.

[150] J. Blomster, O. Lahdenoja, K. Jafarian Dehkordi, *et al.*, "Cardiosignal smartphone application detects atrial fibrillation in heart failure population", *Circulation*, vol. 144, no. Suppl_1, A12517–A12517, 2021.

[151] S. Mehrang, O. Lahdenoja, M. Kaisti, *et al.*, "Classification of atrial fibrillation and acute decompensated heart failure using smartphone mechanocardiography: A multilabel learning approach", *IEEE Sensors Journal*, vol. 20, no. 14, pp. 7957–7968, 2020.

[152] A. Hossein, D. C. Mirica, J. Rabineau, *et al.*, "Accurate detection of dobutamine-induced haemodynamic changes by kino-cardiography: A randomised double-blind placebo-controlled validation study", *Scientific reports*, vol. 9, no. 1, p. 10 479, 2019.

[153] M. M. H. Shandhi, J. Fan, J. A. Heller, M. Etemadi, L. Klein, and O. T. Inan, "Estimation of changes in intracardiac hemodynamics using wearable seismocardiography and machine learning in patients with heart failure: A

feasibility study", *IEEE Transactions on Biomedical Engineering*, vol. 69, no. 8, pp. 2443–2455, 2022.

[154] G. M. Marcus, I. L. Gerber, B. H. McKeown, *et al.*, "Association between phonocardiographic third and fourth heart sounds and objective measures of left ventricular function", *Jama*, vol. 293, no. 18, pp. 2238–2244, 2005.

[155] A. Capucci, L. Santini, S. Favale, *et al.*, "Preliminary experience with the multisensor heartlogic algorithm for heart failure monitoring: A retrospective case series report", *ESC heart failure*, vol. 6, no. 2, pp. 308–318, 2019.

[156] R. Sandler, P. Gamage, M. K. Azad, *et al.*, "Potential scg predictors of heart failure readmission", *Journal of cardiac failure*, vol. 26, no. 10, S87, 2020.

[157] N. Joshi, "The third heart sound.", *Southern medical journal*, vol. 92, no. 8, pp. 756–761, 1999.

[158] N. J. Mehta and I. A. Khan, "Third heart sound: Genesis and clinical importance", *International journal of cardiology*, vol. 97, no. 2, pp. 183–186, 2004.

[159] W. Am, "Systolic time intervals in heart failure in man.", *Circulation*, vol. 37, pp. 149–152, 1968.

[160] F. I. Marcus, V. Sorrell, J. Zanetti, *et al.*, "Accelerometer-derived time intervals during various pacing modes in patients with biventricular pacemakers: Comparison with normals", *Pacing and Clinical Electrophysiology*, vol. 30, no. 12, pp. 1476–1481, 2007.

[161] M. Jafari and N. Ansari-Pour, "Why, when and how to adjust your p values?", *Cell Journal (Yakhteh)*, vol. 20, no. 4, p. 604, 2019.

[162] S. Morra, A. Gauthey, A. Hossein, *et al.*, "Influence of sympathetic activation on myocardial contractility measured with ballistocardiography and seismocardiography during sustained end-expiratory apnea", *American Journal*

of Physiology-Regulatory, Integrative and Comparative Physiology, vol. 319, no. 4, R497–R506, 2020.